The Neural Bases of the Eriksen Flanker Effect: A Model-Based Investigation

Yichen Qian

A thesis submitted in fulfilment of the requirements
for the degree of Master of Science in Psychology
the University of Auckland, 2022.

Abstract

Eriksen's flanker effect is a classic interference phenomenon that has been widely studied in cognitive and behavioural psychology. When a task-relevant stimulus (target) is presented with multiple task-irrelevant stimuli (flankers) surrounding that are incongruent with the target, people tend to make slower and less accurate responses to the task in contrast to the conditions when the target and the flankers are congruent with each other. Despite the extensive investigations, the precise neural mechanisms causing the flanker interference are still under debate. Here, I compared two major approaches that have been widely applied to model the flanker interference: the continuous-flow model (CFM) and the drift-diffusion model (DDM). Although these models have some superficial similarities, they posit different origins for the flanker interference. The CFM suggests that sensory information flows continuously from the sensory cortex into cortical areas responsible for response execution, so that interference can be conceived as competition between response channels. In contrast, the DDM emphasises interference arising at the sensory and cognitive levels. The present study tested these two models with neural measures to evaluate which model provides a more appropriate and neurologically plausible explanation to the flanker interference. For CFM, I recorded the lateralized readiness potential (LRP) as an indicator of relative response activation. In particular, I was interested in whether this would reveal evidence for early activation of the incorrect response when incompatible flankers were displayed (the "Gratton Dip"). For the DDM, I computed "drift rate" as an index of the accumulation rate of sensory evidence. To calculate the drift rate, I flickered the target and flanker stimuli at different frequencies and recorded the resulting steady-state visual evoked potentials (SSVEPs).

Results in the LRP failed to reveal the “Gratton dip” in response to incompatible flankers, but instead revealed a delayed peak in the incongruent condition. On the other hand, the drift rate calculated at occipital electrodes (centred on Oz) for this condition was notably lower than for the compatible condition. Both the delayed LRP peak and the slowed drift rate were significantly correlated with response time. Taken together, these data provide more support for drift-diffusion models in which flanker interference arises at sensory/perceptual levels of processing rather than at the level of response selection.

Acknowledgements

First of all, I would like to thank my supervisor Associate Professor Paul Corballis for his wealth of knowledge and all the insightful ideas enlightened me in the research. I could hardly imagine finishing this research project without Paul's mentorship. I also deeply appreciate all the supports and advice Paul had provided to me in not only this research project but also for my future academic developments. It has been a grateful experience to work with Paul and I feel deeply honored about it.

I would also like to thank my lab mates, Miss Katie Smith, Miss Carley Braddock, Mr. Daniele Scanzi, Mr. Nitish Iyer, and Mr. Eric Rosentreter for all the great supports to me on data collections and the share of knowledge and time to me on conducting data processing, experiment designing, script coding, and statistical analysis. Their brilliant ideas were often enlightening when I was confused by the works.

Another special thanks to Dr. Veema Lodhia and Miss Margaret Francis for their excellent tutorials and consistent, timely, and fully devoted technical supports on EEG equipment practices and troubleshooting. This experiment could never have been achieved without their generous help, especially under the difficulties due to the COVID-19 restrictions.

Most importantly, I would like to thank my family and all my friends who supported me over the whole journey of the master's degree. Their unconditional love is the biggest motivation for me to overcome every difficulty through the past year and in the future.

Table of Contents

1. Introduction

1.1. The Eriksen Flanker Effect.

Introduced by Eriksen and colleagues in the mid-1970s, the noise-compatibility (or "flanker") task is a classic experimental paradigm in cognitive and behavioural psychology. In a standard visual flanker task, participants are presented with a set of stimuli, consisting of a task-relevant target surrounded by multiple task-irrelevant flankers. A judgement response to the target is required with response time and accuracy recorded. The target-flanker congruency is manipulated, creating a congruent condition in which the target and the flankers are compatible with each other (e.g., >>>>>) and an incongruent condition in which the target is incompatible with the flankers (e.g., >><>>). Behavioural results from the flanker tasks typically show longer response time (RT) and lower accuracy in the incongruent trials than in the congruent ones (e.g., Eriksen & Eriksen, 1974). This is commonly termed as "the flanker effect". Over the past half century, the flanker paradigm has been widely used to study various topics, such as cognitive control and perceptual decision making. Ever since its introduction, Eriksen's flanker task has been extensively applied in experimental and clinical research, and the congruency effect was consistently observed with different modifications among various populations (e.g., Erb et al., 2016; Eriksen & Eriksen, 1974; Miller 1991).

Most researchers today concur that the flanker effect reflects competition between the target and the flankers in information processing. Yet, debates remain about the stage(s) of processing at which such conflicts occur, and which neural signatures correspond to such competition. The main point of issue is whether competition arises

early in cognitive processing – perhaps arising in sensory cortex (e.g., Ratcliff & McKoon, 2008; White, Ratcliff, & Starns, 2011) – or at relatively late stages of processing such as at the level of response selection or activation (e.g., Cole et al., 1985; Eriksen & Eriksen, 1974; Gratton et al., 1988).

1.2. The Continuous-Flow Model.

One popular perspective on this topic proposed that the flanker effect is mainly caused by conflicts at the level of response activation. This view is commonly found under the theoretical framework known as the continuous-flow model (CFM) of information processing, which argues that the response system is concurrently influenced by the information inputted from both the target and flankers (Eriksen & Schultz, 1979). An important characteristic of the continuous-flow framework was the absence of a separate decision stage between the stimulus input and response delivery. Instead of having an explicit target recognition before responding, the CFM holds that the streams of sensory inputs in the visual system are constantly fed to the response channels. According to this model, both the target and flankers are processed in the visual system in the early period of perception, leading to activation of both responses (i.e., the response associated with the target and the response associated with the flankers). Later, as cognitive mechanisms like selective attention take effect, the representation of flankers in the visual system will be increasingly suppressed as time proceeds, while the target representation will be enhanced. Consequently, it will allow the activation in the target-related channels to outcompete its flanker-related counterpart and eventually reach a

threshold of overt response evocation. The selective attention process will become more laboring when the target and flankers are incongruent, hence delaying response execution.

1.2.1. Evidence for the CFM.

One of the biggest supporters of the CFM is probably Charles Eriksen himself. In fact, Eriksen had already raised the idea of the continuous flow in his first paper introducing the flanker effect (Eriksen & Eriksen, 1974). In this study, researchers manipulated not only the perceptual congruency, but also, critically, the response compatibility between target and flankers. The incongruent trials were further divided into an incongruent-compatible condition in which the flankers were perceptually different but semantically corresponding to the same response with the target (e.g., "H H H K H H H", both "H" and "K" correspond to right-hand response), and an incongruent-incompatible condition in which the flankers were perceptually different and semantically opposite from the target (e.g., "H H H S H H H", "S" and "H" correspond to left- and right-hand responses, respectively). Behavioural response time (RT) showed that responses in the incongruent-incompatible trials were significantly slower than in the congruent condition, while the incongruent-compatible trials obtained only trivial differences. Eriksen suggested that the RT impairment was mostly determined by the response compatibility of the noises rather than their perceptual similarity, hence the major target-flanker competition must happen between the response channels.

Eriksen's argument was also supported by biophysiological evidence. In 1985, Eriksen and colleagues measured the electromyographic (EMG) waveforms from the two arms when performing a standard flanker task (Eriksen et al., 1985). Results showed increased EMG activities from both the correct-response arm and the opposite in about 40% of all incongruent trials; while only 8% of trials in the congruent condition elicited a similar pattern. This result indicated that both response channels were activated and were competing with each other in the incongruent trials, which accorded to the prediction of the CFM. Later, Coles et al. (1985) replicated Eriksen's finding using a similar flanker task design, but with responses made by squeezing dynamometers with left and right hands. In order to obtain EMG data with better quality, participants in this study were required to squeeze into dynamometers with at least 25% of their maximal force to register responses. Consistent with Eriksen's earlier finding, Coles and colleagues found EMG activities from both hands in the incongruent trials regardless of their overt responses, consistent with the concurrent activation of correct and incorrect response channels. More importantly, the EMG onsets from the incorrect response hand tended to be earlier than from the correct hand, suggesting that the incorrect responses were initially activated but later surpassed by the correct ones in these trials. Similar findings were also reported from further literature using EMG measures (e.g., Coles et al., 1995; Fournier et al., 1997; Davranche et al., 2005; Suarez et al., 2015).

More recently, evidence from response movement trajectory has offered researchers more insights into the dynamics of information flow in the flanker paradigm. Developments in technology over the past two decades have allowed researchers to use new techniques like hand- and mouse-tracking to explore the classic flanker effect (e.g.,

Erb & Marcovitch, 2018; Faulkenberry, Witte, & Hartmann, 2018; Hermens, 2018). Like in the classic flanker task, participants in a typical curvature experiment are presented with target-flanker stimuli with different congruency conditions; but their responses are required to be a continuous stream of movements with trajectory recorded (e.g., hand reaching or mouse sliding) instead of an instantaneous action (e.g., key pressing). It also led to the practical variation that the curvature data is best captured in single-hand responses, while the classic flanker studies relied heavily on results generated from bilateral body movements. Despite the differences from the traditional flanker task, however, the curvature-based findings provided us with a novel perspective of studying the flanker effect with richer temporal and spatial information than usual. For example, Erb and colleagues (2016) recorded the hand movement trajectories from participants performing a modified version of the flanker task. Responses in this study were made by reaching and touching locations corresponding to the target on a touch screen, while the manual movements were traced via electromagnetic sensors attached to participants' right index finger. Results showed that the incongruent trials obtained significantly larger curvatures than the congruent ones in terms of the area under the curve (AUC), indicating deviations from the shortest possible path to the correct response. Critically, these trajectories tended to deviate from the correct response towards the flanker-specific incorrect responses at the initial period of reaching, which met the prediction of the CFM.

1.2.2. Lateralized Readiness Potential and the "Gratton Dip".

The evidence discussed so far seems to support Eriksen's proposal with overt responses or activities observable in the peripheral nervous system (e.g., limbs and hands), but researchers are also interested in understanding the neural bases of the continuous flow and the competing processes that potentially happening in the brain cortices. One of the most potent neurological supports of the continuous-flow model came from a series of work conducted by Gratton and colleagues in the 1980s and 90s using the lateralized readiness potential (LRP). LRP is a lateralization-based event-related potential (ERP), calculated by subtracting the ERPs from the primary motor area ipsilateral to the response hand from the contralateral ones (Eimer, 1998). It is often observed as a negativity over the contralateral hemisphere to the response hand onsets before the execution of overt response (e.g., Deecke et al., 1976; Kutas & Donchin, 1980; Smid et al., 1987). LRP has been considered as reflecting the preparation of response delivery in the primary motor cortex, and typically a negative deflection in the LRP waveform indicates cortical preparation to the correct response hand movement, whereas a positive deflection in LRP indexes activation in the primary motor cortex favouring the incorrect response hand. In addition, the peak amplitude of LRP is believed to reflect the threshold level of cortical preparation needed for overt response generation, and the timing of the LRP peak is often closely associated with the overt response time (Smulders, Miller, & Luck, 2012).

In 1988, Gratton and colleagues replicated Eriksen's work (1985) with both EMG and LRP recorded. In line with the previous findings, behavioural results showed an eminent congruency effect in response time, and EMG excitations were exhibited in both

the correct and the incorrect response hands in the incongruent condition. In addition, researchers observed a slight positivity in LRPs between 150 and 250 ms post-stimulus in the incongruent trials, as illustrated in Figure 1, while the LRP in the congruent condition at the same time window did not show such a pattern. Thus, although the LRP waveform in the incongruent condition returned to negative shortly afterwards, the peak LRP amplitude was notably weakened in contrast to its congruent counterpart. Given the general understanding of the nature of LRP discussed above, this positive waveform in the incongruent condition was believed to reflect a slight motor preparation towards the incorrect response hand shortly after the stimulus onset when flankers were conflicting. This result fit perfectly with the continuous-flow model (CFM) of information processing which predicted that the incongruency could misguide the subject to slightly activate the false response at the early stage of processing when the perceptual presence of the flankers was dominant. Such misguidance could be overcome later when selective attention inhibits the distractions, but the preparation, and consequently the execution of the response would be lagged. It also indicated that the interference from the conflicting flankers could be observed, at least partially, in the response channels in the primary motor cortices even at an early stage after stimulus onsets. They further suggested that information from the stimulus array could be continuously accumulated and made available to the response system (Gratton et al., 1988). Gratton and colleagues replicated this finding in another study in 1992, in which they consistently found the early positivity in LRP in incongruent trials even under various manipulations on trial sequence, global probability, and cueing validity (Gratton, Coles, & Donchin, 1992). Since this positivity found by Gratton in LRP was presented as a down-facing “dip” in the old-school ERP

imaging custom, this pattern has frequently been referred to as the “Gratton dip” in the literature.

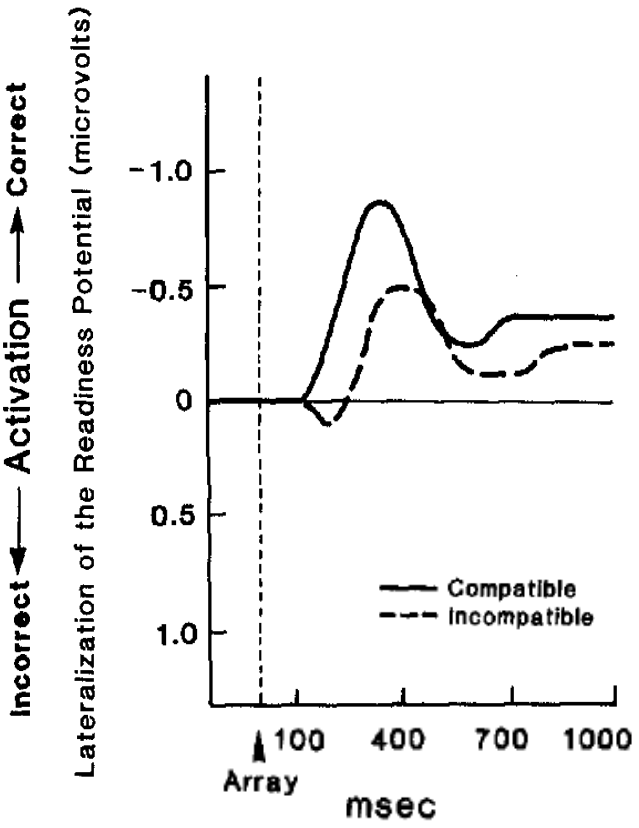

Figure 1. Lateralized readiness potential (LRP) waveform (adapted from Gratton et al., 1988). LRP amplitudes were measured in microvolts. A slight positivity in LRP was found at the early stage (150 - 250 ms) after the stimulus onset in the incongruent (dashed) condition but not in the congruent (solid) condition, which was later known as the “Gratton dip”. The peak and mean amplitude of LRP was weakened in the incongruent condition in contrast to the congruent one.

1.3. The Drift-Diffusion Model.

In parallel to the development and exploration of the continuous-flow model, many other researchers have investigated the flanker effect from a cognitive decision making perspective. The diffusion model is probably one of the most representative schools among them. Emerged from the longstanding aim in cognitive psychology of building mathematically computable models of decision, diffusion models are generally designed to be applied to all rapid sensory tasks involving simple two-alternative forced choices (2AFC), including the flanker task (Ratcliff, 1978; Ratcliff & McKoon, 2008; Ratcliff et al., 2016), but some recent works also showed the potential of fitting the diffusion model to the tasks with continuous outcomes (Harlow & Donaldson, 2013; Zhou et al., 2021). While the name of diffusion model can be generally referred to the entire class of models sharing a common theoretical framework (e.g., Busemeyer & Townsend, 1993; Diederich & Busemeyer, 2003; Gold & Shadlen, 2001; Laming, 1968; Link & Heath, 1975; Palmer, Huk, & Shadlen, 2005; Ratcliff, 1978, 1981, 1988, 2002; Ratcliff, Cherian, & Segraves, 2003; Ratcliff & Rouder, 1998, 2000; Ratcliff & Smith, 2004; Ratcliff, Van Zandt, & McKoon, 1999; Roe, Busemeyer, & Townsend, 2001; Stone, 1960; Voss, Rothermund, & Voss, 2004), the present study will primarily discuss the drift-diffusion model (DDM) proposed by Roger Ratcliff (1978), which is the most representative one.

1.3.1. DDM Parameters.

Unlike the CFM which highlights the competition between the two motor response channels, the DDM approach tends to attribute the flanker congruency effect to interference in sensory processing and conflicts at the stage of internal decision making. According to the DDM, decision making in 2AFC tasks involves a noisy accumulation of perceptual information, or the cognitive "*evidence*" favouring one choice out of the two. The evidence is assumed to start from a certain "starting point" (z) and gradually accumulate as a function of time until hitting the "boundary" (a), a threshold amount of evidence supporting one of the decisions. Depending on the noisiness of perceptual inputs at each time point, the mathematical value of the accumulated evidence could go either positively or negatively respective to the accumulation starting point, in other words "drift" towards or be "diffused" away from the boundary of the correct choice, respectively. When the accumulation reaches the threshold of the wrong choice, an incorrect response will be made. The speed of evidence accumulation is labelled as the "drift rate" (v). The accumulation of evidence is proposed to take place in one or more accumulators, which is an important cognitive structure proposed in DDM. In contrast to the continuous-flow model (CFM), the diffusion model assumes an explicit decisional process happening at the sensory and cognitive level, and it is distinct from non-decisional factors or errors (T_{er}), such as the time needed for response preparation and execution (Ratcliff & McKoon, 2008). A graphic illustration of a simulated drift-diffusion process is presented in Figure 2. In a way, decision making under the diffusion framework is considered as an all-or-none process such that one would make a decision only when the accumulated evidence reaches the threshold of one response. Together, a

combination of these parameters determines the behavioural outcome of a trial. Ceteris paribus, a higher drift rate, a smaller disparity between the starting point and the boundary, and a shorter non-decisional time would lead to a faster response.

The diffusion models were designed to explain the data and patterns from 2AFC tasks, mostly at the behavioural level, such as the distributions of response time, error rate, and the speed-accuracy tradeoff effect. Typically, the DDM parameters are estimated via optimization algorithms based on the behavioural response time and accuracy and their distributions (e.g., Ratcliff & Tuerlinckx, 2002). Each of these parameters is assumed to reflect an independent cognitive aspect in decision making and could be systematically affected by some experimental manipulations. For example, empirical findings suggested that drift rate (v) could be influenced by the task difficulty, such that easier trials correlated with higher drift rates. Individuals with relatively high general intelligence also tended to score highly in drift rate on average (Ratcliff et al., 2010, 2011). On the other hand, the separation between two response boundaries (a) was believed to be closely related to the speed-accuracy tradeoff. Several reports indicated that an accuracy-highlighting instruction could lead to a greater threshold value, and vice versa (Ratcliff & McKoon, 2008; Voss et al., 2004). The starting point (z) was considered to reflect a biased tendency favouring one choice over the other, and it could be affected by factors such as the reward history (Voss et al., 2004), trial sequence (Nguyen, Josić, & Kilpatrick, 2019), probabilistic frequency (Leite & Ratcliff, 2011), and relative valences (Voss, Rothermund, & Brandtstadter, 2008). Lastly, several experiments showed that the non-decision time (T_{er}) could increase if the motor response is prolonged, for instance changing from a key-pressing to a finger movement response (Voss et al, 2004). Other

factors including age, bilingualism and grey matter volumes in the prefrontal cortex also tended to correlate with T_{er} (e.g., Ong et al., 2017; Spaniol, Madden, & Voss, 2006; Spaniol, Voss, & Grady, 2008; Soares et al., 2019).

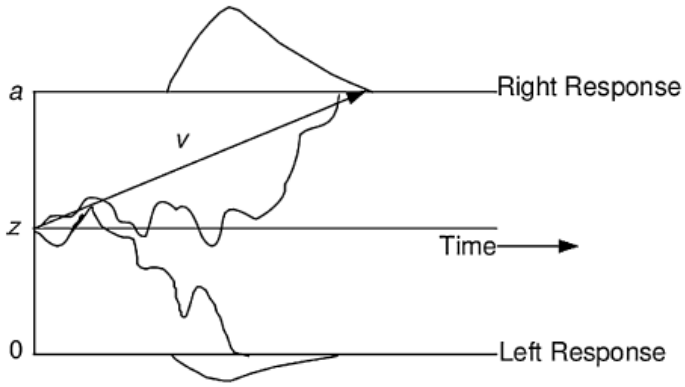

Figure 2. Hypothetical standard drift-diffusion process (adapted from White et al., 2011). Noisy evidence from the stimulus inputs accumulates over time from a starting point value *z* at a drift rate of *v*. A decision would be made as soon as the accumulation reached one of the two thresholds, *a* and 0, and eventually lead to the execution of the corresponding response.

1.3.2. Neural Correlates of DDM.

While the concept of the diffusion model has been proposed for half a century, for quite long its influence remained in a relatively limited scope due to its huge demand of computation power for iterative calculations and simulations. So far most of the diffusion model fittings and simulations were based on simple behavioural data of response time and accuracy, while its compatibility with more complicated neurological data was largely unclear. Fortunately, favoured by the rapid development in computer science and machine learning technology, an emerging number of works in recent years suggested that some neural signatures might be associated with the drift-diffusion process. For example, Shadlen and colleagues conducted a series of studies in which they recorded the neuron firing rate when monkeys were performing motion discrimination tasks with eye-movement responses (Gold & Shadlen, 2001; Huk & Shadlen, 2005; Kiani, Hanks, & Shadlen, 2008; Roitman & Shadlen, 2002). Their results showed monotonically increased firing rate in the lateralized intraparietal cortex (LIP). Critically, the timing of the firing rate reaching a threshold value strongly predicted the behavioural response time and accuracy, which was consistent with the assumption of bounded evidence accumulation in the diffusion model. Other studies using a similar paradigm also reported increasing firing rates in cells from the frontal eye field (FEF) and superior colliculus (SC) with their buildup rates correlated to the drift rate parameter in DDM (Hanes & Schall, 1996; Heekeren, Marrett, & Ungerleider, 2008; Ratcliff, Cherian, & Segraves, 2003). However, conclusions from these studies remained debatable, since the LIP, FEF and SC regions were also closely related to saccadic movement control (Colby et al., 1996; Glimcher & Sparks, 1992; Gnadt & Andersen, 1988; Horwitz & Newsome, 1999, 2001; Krauzlis &

Dill, 2002; Platt & Glimcher, 1997; Sparks, 1999). Whether activities in these regions reflect a real drift-diffusion process or just a mere response preparation, in other words a saccadic version of the "Gratton dip", was not clearly differentiated. On the other hand, works based on functional magnetic resonance imaging (fMRI) and repetitive transcranial magnetic stimulation (rTMS) suggested that the left dorsolateral prefrontal cortex (dlPFC) was also associated with perceptual decision making, but the temporal dynamics of accumulation were difficult to examine in these experiments (e.g., Basten et al., 2010; Philiastides et al., 2011).

In comparison, electroencephalography (EEG) tended to be a more ideal non-invasive technique applicable to human objects to capture the temporal dynamics in decision-making. Several EEG-based components had been found to be potentially related to the drift-diffusion process. For instance, O'Connell, Dockree and Kelly (2012) identified a centro-parietal positivity (CPP) which increased in amplitudes as a function of stimulus exposure time and reached maximums at response execution. This signal was general to the sensory modality of the stimuli and was observed regardless of whether an overt response was presented or not, indicating its independence from the motor preparation. This finding was replicated in their later study with a motion detection paradigm (Kelly & O'Connell, 2013). Some other works using on single-trial EEG analysis also claimed that some positive waveforms sourced from the parietal regions, onset at about 300 ms post-stimulus, was correlated with the drift rate in the diffusion model (e.g., Nunez, Vandekerckhove, & Srinivasan, 2017; Philiastide, Ratcliff, & Sajda, 2006). However, even though many of these studies claimed their results as potential neural correlates of the drift-diffusion processes, strictly speaking these findings were

merely EEG signals that shared some common characteristics (e.g., hit-to-boundary amplitude) with the hypothetical drift-diffusion processes. No computational fitting of these neural data to the DDM framework was attempted with these neurological data. Thus, correlating these signals with the DDM parameters like the drift rate was also methodologically problematic, because the mathematical values of these parameters were often reversely estimated by the algorithms to best fit the behavioural response time and accuracy, so that the reported correlations might actually reflect the associations between neural signals and behavioural performances rather than the drift-diffusion processes per se. As we can see, few studies so far have managed to build a clear, direct link between the theoretical DDM and the actual biophysiological data, and the neural bases of the drift-diffusion process in humans remain largely unexplored.

1.3.3. DDM of the Flanker Task.

Enormous literatures have now shown that the diffusion models make a good account for various types of 2AFC tasks such as the motion discrimination task (Ratcliff & McKoon, 2008), Stroop task (Alos-Ferrer, 2018), face recognition task (Philiastides, Ratcliff, & Sajda, 2006), lexical decision task (Wagenmakers, Ratcliff, Gomez, & McKoon, 2008), and recognition memory task (Arnold, Broder, & Bayen, 2015). Not surprisingly, DDM has also been applied to explain the flanker congruency effect. In 2011, White and colleagues made a comprehensive review of the flanker congruency effect under the DDM framework. In particular, they suggested that a diffusion model

with a shrinking spotlight assumption of selective attention would provide the best fit for the behavioural performance from flanker tasks (White, Ratcliff, & Starns, 2011).

According to the shrinking spotlight DDM, the evidence accumulation was hugely shaped by the temporal dynamics of attention distributed to each item of the stimulus array. For an incongruent trial, the attention was assumed to be normally distributed to the entire stimulus array at the initial stage of exposure, so that the overwhelming flankers would occupy a large proportion of attentional resources in contrast to the target. The accumulated evidence was therefore predicted to be attenuated or even deviated towards the incorrect decision boundary. As the trial continued, selective attention would gradually take effect and become concentrated on the target while the flanker presence was suppressed, which would eventually drive the accumulation towards the boundary of the correct choice at a late stage. This potential "U-turn" in the direction of evidence accumulation meant more perceptual input and longer exposure time needed to reach the threshold, which explained the delayed response in the incongruent condition. If the deviated accumulations reached the incorrect choice boundary before the selective attention took place, response errors were made. This interpretation also implied that the competition causing the flanker effect happened at the level of sensory evidence accumulation and was largely controlled by the attention dynamics. A graphic illustration of the shrinking spotlight DDM is shown in Figure 3. White and colleagues examined the fitness of this model with the behavioural data under various manipulations in response bias, global probability, speed-accuracy tradeoff, and stimulus configuration. Their results suggested that the diffusion model with a shrinking

attention spotlight seemed to provide a plausible explanation for the flanker congruency effect in all manipulated conditions.

More importantly, White and colleagues proposed a specific formula in this study to compute the evidence accumulation speed based on the input strengths and the attention distribution. According to White et al (2011), the drift rate (v) in a trial would change as a function of time and could be calculated as:

$$v(t) = p_{\text{target}} \times a_{\text{target}}(t) + \sum p_{\text{flanker}} \times a_{\text{flanker}}(t)$$

meaning that the decision evidence sampled at each time point equaled the sum of the perceptual input strength (p_i) of each item (target or flankers) weighted by their corresponding, time-varying attention allocation ($a(t)$). Although White et al. never managed to actually compute the drift rates using this formula due to the difficulty in quantifying the changing attention under their experimental design, their proposal still introduced us a potentially feasible way to proactively measure the DDM parameter instead of relying on the reverse estimations from the behavioural performance. For this reason, the shrinking spotlight DDM became one of the major models investigated in the present study, and the use of the drift rate formula was highlighted.

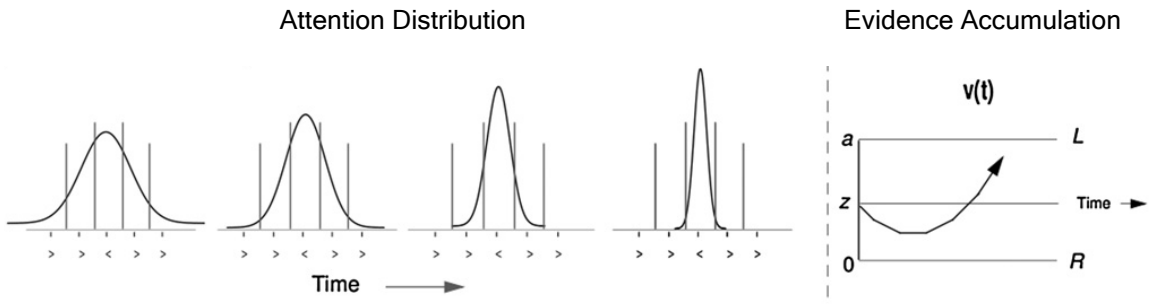

Figure 3. Evidence accumulation in the shrinking spotlight drift-diffusion model (adapted from White et al., 2011). Attention was normally distributed to each item of the stimulus array at the start of trial presentation but gradually became concentrated over time. Correspondingly, the accumulated cognitive evidence was initially more favouring the flanker-related decision but returned to the target-related decision as attention getting focused.

1.4. The Present Study.

1.4.1. Continuous-Flow Model vs. Drift-Diffusion Model.

Despite the common origins of the continuous-flow model (CFM) and drift-diffusion model (DDM) and their largely parallel development, few studies have directly compared them or sought possible points of connection between them. Development in relative isolation has led to some major differences between the two models. The CFM explains the flanker-congruency effect from a response perspective, and considers the effect as an outcome of competing activation between response channels. In contrast, the DDM explains the phenomenon in a decision-making context, and highlights competition at sensory and cognitive levels during evidence accumulation. In this context, prolonged responses in incongruent trials are due to delayed decision making. In practice, studies performed in a CFM context have often highlighted the use of biophysiological evidence such as EMG and LRPs; whereas the DDM-based studies have relied largely on mathematical modelling and simulations. It also led to a situation in which the CFM has a relatively simple theoretical structure, but specific and quantifiable indexes for experimental verification - and is hence more strongly supported by empirical evidence – whereas the DDM has a more precisely developed theoretical framework but is relatively weak in terms of empirical support. Even though some critical findings from CFM studies are sometimes cited in the DDM literature, and vice versa, in most cases they have still been underestimated with only a subordinate role in contrast to the main arguments. For instance, the finding of the "Gratton dip" (Gratton et al., 1988) was mentioned in a DDM-based study of flanker-task performance by White et al. (2011) as an example of the nondecision activities (i.e., error) that separated from cognitive

decision making and could not be well accounted by the DDM. Although they recognized that nondecision motor preparation might also be sensitive to the flanker congruency under certain conditions as adaptations, overall the nondecision errors were assumed to remain relatively constant and would not become the primary reason causing the flanker congruency effect.

On the other hand, even with the abovementioned differences in theoretical frameworks and empirical traditions, the CFM and DDM also share some remarkable similarities with each other. Firstly, both models posit that stimulus inputs function as continuous information streams that are constantly influencing the competition between target and flankers, albeit at different levels. Secondly, both models recognize the critical role of selective attention as a gradual concentration process favouring the presence of the target while suppressing the interference from flankers. Thus, both models assume some type of accumulation of the influence from stimulus inputs at some level prior to the commission of an overt response. Such stimulus influence is conceptualised in the DDM as the accumulation of cognitive evidence towards the hypothetical thresholds corresponding to the two alternative decisions. In the CFM, such influence was considered to be accumulated in the motor response channels in the form of the lateralized readiness potentials (LRPs). These characteristics jointly lead to similar predictions of the misled incorrect decisions or the deviated activation towards incorrect response at the early stages in the incongruent conditions.

The driving questions of the present study arise from these discrepancies and similarities: Which model best explains the flanker congruency effect? What are the connections, if any, between these two models? Could it be possible that the “Gratton

dip" actually reflects something similar to the drift-diffusion process? Answering these questions would give a more comprehensive view of the processes occurring during the flanker task, and more generally in other behaviours involving conflict between alternative decisions. To answer these questions, an experiment that could be used to examine both the CFM and the DDM needs to be conducted, with effective comparisons and contrasts of the explanatory power between the two models.

As mentioned earlier, the CFM can be tested relatively easily via measurements such as the lateralized readiness potentials (LRPs). In contrast, examining the DDM at the neurophysiological level entails more ambiguities. A major challenge for the experiment design therefore fell on how to effectively evaluate the DDM using neural signals. Given the drift rate formula proposed by White and colleagues (2011) based on the perceptual input strength weighted by distributed attention, one potential solution to this challenge used in the present study was to track the streams of stimulus inputs. Specifically, I was interested in how the target and the flankers are represented in the visual cortex, and how they vary and interact with each other over the course of the task. This information would help us to transfer the drift rate from a hypothetical parameter into a measurable index with neural foundations. In animal experiments, such stimulus tracking is usually achieved via the single-cell recording technique as time series neural signals provide plentiful temporal information (e.g., Gold & Shadlen, 2001; Huk & Shadlen, 2005). As a non-invasive substitute applicable in normal human subjects, I took advantage of a phenomenon called "frequency tagging" to track the representation of the two input streams.

1.4.2. Frequency Tagging.

Frequency tagging is based on the steady-state visual evoked potential (SSVEP). This is a special type of visual evoked potential induced by periodically changing stimuli at a constant rate. Numerous observations showed that ERPs generated by such stimuli are highly stable in amplitudes and coherent in phase, in other words in a "steady state" (Adrian & Matthews, 1934; Regan, 1966). Importantly, the power spectrum of these visual evoked signals in the frequency domain tends to be strictly related to the stimulation rate. For example, when a stimulus flashing at 10 Hz is presented, the frequency spectrum of the corresponding SSVEPs typically also shows enhancement at 10 Hz (Heinrich, 2010). Empirically, SSVEP is best observed at the occipital electrode sites (often Oz) with stimulus flashing at a rate between 3 and 20 Hz (e.g., Fawcett et al., 2004; Di Russo et al., 2007; Muller et al., 1997; Srinivasan, Bibi, & Nunez, 2006), but several works have also reported SSVEPs at extremely low and high frequency ranges in other cortical regions involving higher-level sensory processes such as motion detection and facial recognition (e.g., Alonso-Prieto et al., 2013; Herrmann, 2001; Norcia et al., 2002; 2015; Regan & Regan, 1988).

Given its stimulus-signal symmetricity, frequency tagging allows researchers to simultaneously measure the visual processing of stimuli presented at different frequencies. A typical frequency-tagging task involves two or more sets of stimuli that are structurally (temporally or spatially, depending on the research question) isolated from each other, with each stimulus set flickering at a unique rate. Conceptually this enables us to extract the cortical responses corresponding to each stimulus set from the spectral power structure of the EEG signal (Tononi et al., 1998). This method has been

proven to be highly effective in studying the temporal dynamics of attention allocation and visual processing. For instance, Morgan and colleagues (1996) recorded the evoked potential from the bilateral primary visual cortices when participants were presented with a string of letters on one side of the screen and a string of numbers on the other half. The two strings were flashed at 8.6 and 12 Hz, respectively, and the participants were instructed to attend to the left or right by a spatial cue at the beginning of each trial. Their results showed that signals collected from the visual cortices were strictly frequency tagged to the stimulus flashing rate presented in contralateral visual hemifields. Thus, the SSVEPs were notably enhanced when the corresponding hemifield was attended to in contrast to the unattended trials. A subsequent fMRI study also connected this effect in SSVEPs to the level of blood-oxygen-level-dependent (BOLD) activities in the lateral occipital regions (Hillyard et al., 1997).

Visual processes can also be analyzed via frequency tagging even when multiple stimuli are spatially overlapping or embedded in one another. In a study conducted by Muller and Hubner (2002), participants were presented with a large letter, flashing at one rate, with a small letter embedded in the centre, flashing at some other rate. Participants were asked to recognize either the large or the small letter while ignoring the other. Recordings from occipital and parietal regions showed that EEG signals were well tagged to the small letter frequency when being asked to focus on the centre, suggesting that SSVEP could be observed even when the inducing stimulus was surrounded by distractors tagged with a different frequency. More interestingly, trials with instruction to attend to the large surrounding letters also obtained strong SSVEPs, indicating that attention could be formed in a “doughnut shape”. In another study, Muller et al. (2006)

presented the participants with red and blue dots that were randomly distributed on the screen with overlap. The red dots were consistently flickering at one rate and the blue ones were flickering at another. The participants were instructed to attend to either set at the beginning of each trial. SSVEP amplitude enhancements in the occipital regions were found for the attended stream without notable interference from the unattended stream frequencies. Together, these findings demonstrated the reliability of the frequency tagging method even with multiple overlapping stimuli.

1.4.3. Frequency Tagging Application in the Present Study.

In the present study, the multiple input frequency tagging method was applied to trace the processing of the target and flankers. I designed a variant of the flanker task with the central target and the surrounding flankers flashing at two distinct rates. The choice of flashing rates was determined based on the empirically optimal range (Norcia et al., 2015), the capabilities of available equipment, and the compatibility with other task features. Thus, unlike the fully spectrum- or time-series-based approaches commonly seen in the SSVEP literature, a time-frequency analysis was employed to integrate the information from both the time and frequency domains. This would allow us to better visualize and explore the interactions between the two frequency-tagged streams over time.

Despite the intuitive appeal of this approach, I identified some critical problems in the first several test versions of the experiment. Traditionally, SSVEPs are observed under relatively long stimulus exposures, say 1000 or 2000 ms, to allow adequate time

for the frequency-tagged modulations to reach a stable steady state that can be reliably extracted from the ongoing EEG signal (e.g., Morgan et al., 1996; Muller et al., 2006). In sharp contrast, the standard flanker paradigm requires that responses be committed as fast as possible, so that typical trials in flanker tasks are shorter than 500 ms on average (e.g., Gratton et al., 1988; White et al., 2011). While theoretically the effect of frequency tagging should always exist as long as the exposure time exceeded the length of one full cycle of stimulus flashing, observing such effects with relatively short stimulus exposure can be quite difficult in practice. Thus, EEG signals shortly after the stimulus onset usually contain various components in the time-frequency domain, such as some notable alpha-band (8-15 Hz) desynchronizations and theta-band (4-8 Hz) synchronizations which could be universally observed in almost all kinds of visual perception tasks (Klimesch et al., 2011; Petsche et al., 1997; Sauseng et al., 2005). These components are likely to be mixed with tagged modulations in the time-frequency data even though they are not induced by the flickering of the stimulus. In other words, it would be hard to know whether an observed time-frequency power at X Hz was purely due to the X-Hz-flickers or was induced by other neural mechanisms. To address these issues, I also included trials with standard static stimuli in the experimental design as baseline comparisons. The working assumption was that if both flashing and static stimulus arrays generate the universal components, but the additional frequency-tagged modulations could only be found in the flashing trials, then subtracting the non-flashing time-frequency data from the flashing ones would leave us the net effect of frequency tagging.

In the present experiment, I used one static and two flashing conditions. Participants were asked to respond to the direction of the target by key press. Behavioural

response time, accuracy, and EEG signals were recorded during the task. No explicit instructions for emphasising the response speed or accuracy were given. The flankers could be either congruent or incongruent to the target. EEG data was used for both time-locked ERP and time-frequency analyses. The primary indicator for the continuous-flow model (CFM) examined in this study was the lateralized readiness potential (LRP), whereas the drift rate calculated based on the time-frequency data was the main subject of examination for the drift-diffusion model (DDM). If the flanker congruency effect is more consistent with predictions of the CFM, the "Gratton dip" should be replicated in the LRP waveforms, with also attenuated amplitude and delayed peak latency in the incongruent condition in contrast to the congruent condition, and such pattern should also be mirrored in behavioural responses (RTs). . Alternatively, if the DDM makes a better prediction about the flanker congruency effect, the drift rates in the incongruent condition would be lower than in the congruent condition, and correlations should also be observed between drift rates and RTs

2. Methods

2.1. Participants.

32 adults were recruited for the present experiment via posters spread around the campus of the University of Auckland. 4 participants were excluded from the analysis due to either accidental interruptions during the data collections or overall accuracies lower than a predetermined standard (< .85), left us 28 samples available for further analyses, including 13 females and 15 males. 21 of the subjects were right-handed. All participants reported normal or correct-to-normal vision and were aged between 18 and 36 (M = 22.458, SD = 3.426). An information sheet stating the research objectives and interests attached with a written consent form was provided to each participant before the experiment. All research protocols were approved by the University of Auckland Human Participants Ethic Committee. An NZD 20 gift card was awarded to each participant after the experiment for their participation.

2.2. Stimulus.

All experiments were conducted in a darkened electrically shielded room in the School of Psychology at the University of Auckland. An ASUS VG278HE - 3D LCD monitor was used for the experiments with a screen size of 1920 × 1080 pixels and a maximal refresh rate at 144 Hz.

Participants were seated at 57 cm in front of the screen during the experiments. Each trial started with a cross (‘+’) fixation mark presented at the centre of a homogenous

black background (RGB = [0,0,0]) for a warning interval, lasting randomly between 900 and 1800 milliseconds (ms). The fixation mark obtained 1º visual angle in size at this distance. The fixation would flash briefly (onset = 1/3 of the length of the warning interval) to signal the start of the trial and drag participants' attention to the screen centre. A horizontal array of 5 white triangles (RGB = [255, 255, 255]) was then displayed at the screen centre. Each triangle was subtended to 3º in visual angle and the entire array was 16º in size. Each array consisted of 1 "target" triangle in the centre and 4 "flankers" triangles on the left and right. The top vertex of each triangle could point either to the left (L) or to the right (R). Participants were instructed to make a judgement on whether the "target" was pointing to the left or to the right via keyboard pressing ('z' and '/', respectively). The stimulus array would stay on the screen until either a response was made, or a time-limit (5000 ms) was reached, whichever was achieved first. After the task stimuli disappeared, an inter-trial interval (ITI) of 1000 ms with a static 1º cross fixation was presented before the next trial starts. A graphic illustration of the stimulus display is presented in Figure 4.

Within a trial, the direction of all "flankers" were always consistent with each other, while the direction of the "target" could be either congruent ("CO") (e.g., ▶▶▶▶▶) or incongruent ("IN") (e.g., ▶▶◀▶▶) with the surrounding "flankers". Thus, the "flankers" and the "target" simultaneously flashed on different frequencies to produce discriminable SSVEPs. 3 flicker conditions were applied in the present experiment: 24Hz target/18Hz flankers ("A"), static target/static flankers ("B"), and 18Hz target/24Hz flankers ("C"). The choices of flicker frequencies were made based on both the empirical findings from SSVEP literature and the hardware limitations. The flashes were achieved via stimuli

on/offset switches using 2 square-wave functions of frame numbers (i.e., 24 Hz = 6 frames per cycle; 18 Hz = 8 frames per cycle). Together, the combination of flicker pairing (A/B/C) and congruency (CO/IN) created 6 overall stimulus conditions ("ACO", "AIN", "BCO", "BIN", "CCO", "CIN"). A complete experiment session consisted of 20 task blocks, each containing 48 trials, giving 960 trials in total. Trials from all 6 conditions were equally likely to be presented in each block and throughout the experiment (i.e., 160 trials per condition). Each condition contained equal amount of left- and right-response trials. A participant-controlled break interval was provided at the end of each block, and an experimenter-controlled pause was given at the end the 10th block for impedance checks for the EEG data collection.

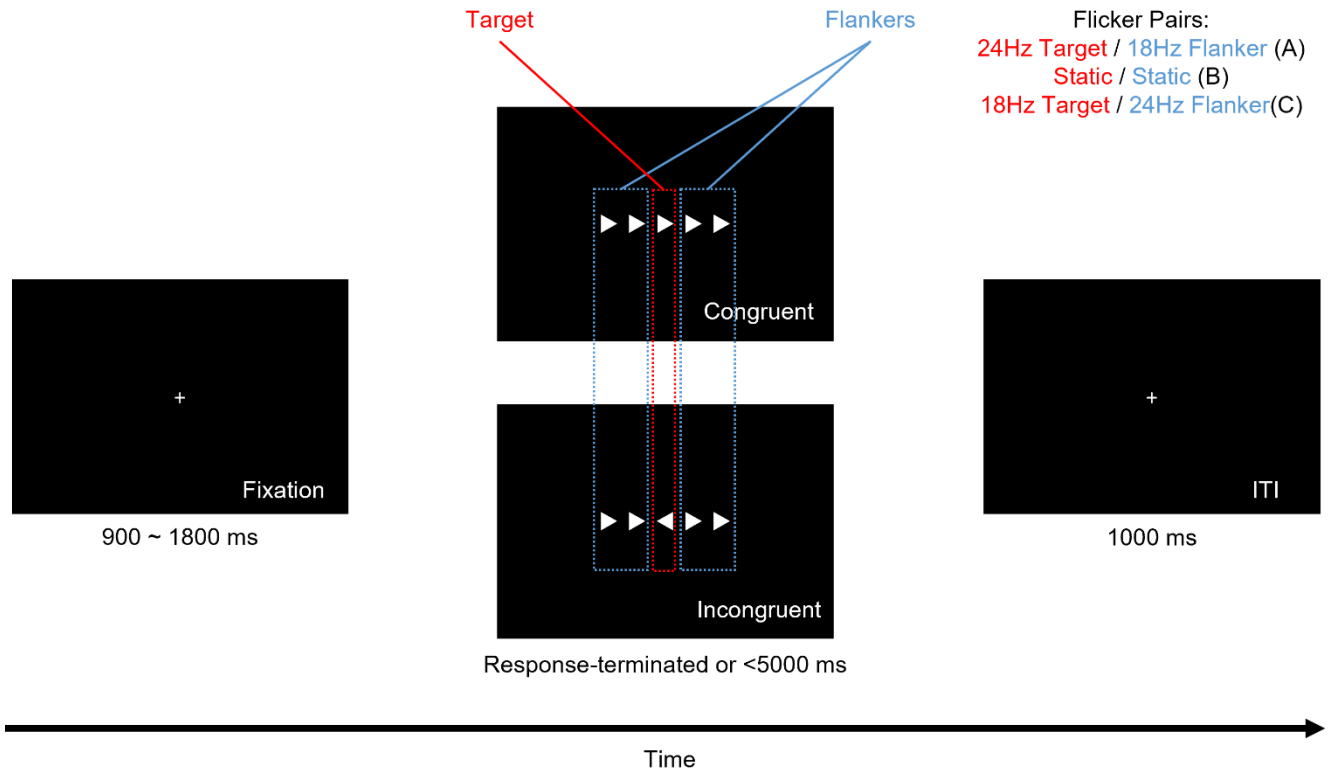

Figure 4. Illustration of the stimulus presentation procedure. A typical trial will start with a fixation lasting randomly between 900 and 1800 ms, followed by a stimulus array consisted of 1 target in the centre and 4 flankers on the surroundings. Target can be either congruent or incongruent with the flankers. The target and the flankers will flash at different rates depending on their assigned flicker condition. The stimulus array presentation will be terminated either when a response was made or when the presentation time exceeded 5000 ms. A 1000-ms-long inter-trial interval (ITI) will be given at the end of each trial.

2.3. Electroencephalographic Recording and Preprocessing.

The electroencephalography (EEG) recordings were conducted in an electrically shielded room (IAC Noise Lock Acoustic - Model 1375, Hampshire, United Kingdom) using 128-channel Ag/AgCl electrode nets (Tucker, 1993) from Electrical Geodesics Inc. (Eugene, Oregon, USA). EEG was recorded continuously (1000 Hz sample rate; 0.1-400 Hz analogue bandpass) with Electrical Geodesics Inc. amplifiers (400-MΩ input impedance). Data was acquired using common vertex (Cz) as a reference. Electrode impedances were kept below 40 kΩ, an acceptable level for this system (Ferree, Luu, Russell & Tucker, 2001), and measured both prior and halfway through the experiment.

EEG data was preprocessed using EEGLAB toolbox (Delorme & Makeig, 2004) written for MatLab (The MathWorks Inc., Natick, Massachustess). The raw EEG data was first down-sampled to 250 Hz, then filtered between 0.1hz and 50 Hz using a finite impulse response band-pass filter, and finally re-referenced to the average. Line noises and artefacts were inspected and removed from the data via the CleanLine (Mullen, 2012) and Artifact Subspace Reconstruction (ASR) (Miyakoshi & Kothe, 2013) functions in EEGLAB. Discarded channels were interpolated. The continuous data was segmented into epochs starting from 1000ms prior stimulus onsets to 1696ms after stimulus presentation. The time-zero points were synchronized to the onset of the stimulus array. Independent Components Analysis (ICA) was then applied to the segmented data using the PICARD algorithm (Ablin, Cardoso, & Gramfort, 2018a, 2018b) in EEGLAB, and components that were identified as non-brain artefacts were rejected.

2.4. Event-Related Potential and Lateralized Readiness Potential Analyses.

EEG data cleaned by the preprocessing pipeline were subjective to further event-related potential (ERP) analysis. Waveforms from each single trial were corrected by subtracting the average amplitudes within the baseline time window. For the present study, the primary research interest focused on the stimulus-locked neural activities, so the ERP baseline window was defined as from 600 to 100 ms pre-stimulus. To explore the neural activities happening in the sensory system, the ERP analyses in the present experiment focused on the waveforms from 3 central-posterior sites of electrode: Oz, Pz, and CPz.

The lateralized readiness potential (LRP) was measured in the same method as in the original literature to effectively replicate the "Gratton dip" (Gratton et al., 1988; 1992). ERP waveforms collected from C3' and C4' were classified as contralateral and ipsilateral to the correct response hand depending on the stimuli presented in a given trial. For instance, if the correct response of a trial is right-hand pressing, ERP from C3' will be labelled as contralateral and C4' will be ipsilateral. LRPs were then calculated by subtracting the ipsilateral ERP from the contralateral ones.

Each ERP/LRP component was examined in the mean amplitude over its defined time windows. For some components (e.g., LRP), additional features including the peak latency ("Latency"), peak amplitude ("Maximum"), and the component duration ("Duration") were also tested to better characterise the data after visually inspecting the waveforms. The peak of a component was defined as where its amplitude reached the

maximum or minimum, while the duration of a component was defined as the interval where the waveform exceeded 1/3 of its peak amplitude (Picton et al., 2000).

2.5. Time-Frequency Analysis.

Time-frequency analyses were also applied to the preprocessed EEG data. Spectral power was estimated by a complex Morlet wavelet transformation in the frequency range between .5 to 30 Hz and at .5 Hz precision, using the MNE-Python package (Gramfort et al., 2013). Like in the ERP analysis, the baseline time windows were defined at between pre-stimulus 600 to 100 ms for the stimulus-locked data. To allow possible cross-frequency comparisons and calculations, a relative approach of baseline correction was used for the time-frequency analysis, and all time-frequency powers were quantified in the unit of percentage changed from the baselines (TF%) (e.g., Grandchamp & Delmore, 2011; Hu et al., 2014). While no specific time window of interest was determined before the experiment given the exploratory nature of the present research, the main analysis focused on the time-frequency dynamics that happened after the stimulus onset and before the response implementation. The frequencies of interest were mainly focused on 18 and 24 Hz, which were the flashing rates of the flickers.

As noted in previous sections, one challenge with the current experiment design was the difficulty of dissociating frequency-tagged modulations from other components generally in wider frequency bands. In other words, power changes on a specific frequency, says 18 Hz, might not only be due to the flickers but also other general neural activities such as beta-band synchronizations. This issue is worsened by the fact that the

effect of frequency tagging tended to be weak under relatively rapid stimulus exposures (Norcia et al., 2015). To better dissociate the frequency-tagging effects, the time-frequency data from the stimulus-flashing conditions (ACO/AIN/CCO/CIN) were then subtracted by corresponding stimulus-static (BCO/BIN) conditions, with congruency corresponded, to calculate the amount changed from the static baselines, or called the time-frequency differences (TFDs). Significant TFDs found at the frequencies tagging to the target/flankers would be considered as reliably reflecting the presences of the stimulus flashing on the corresponding rates.

2.6. Drift-Diffusion Model Analysis.

A simplified drift-diffusion model (DDM) modified based on White et al.'s work (2011) was used for the present study. The main DDM analysis in the present study focused on the drift rate, calculated using the formula below:

$$v(t) = p_{\text{target}} \times a_{\text{target}}(t) + \sum p_{\text{flanker}} \times a_{\text{flanker}}(t)$$

The overall drift rate (v) was then calculated by averaging the $v(t)$ within a certain time window. The value of p_i represented the perceptual input strength of each item (target or flankers) and could be positive or negative in relative to the correct response of the trial. p_{flanker} would be positive in a congruent trial but negative in an incongruent one; whereas p_{target} would always be positive. Since the target and the flankers were completely identical in size, color, and luminance, an equal absolute value for each of item that could be standardised to 1 in calculations was assumed. The time-varying attention $a_i(t)$ for

target and flankers were calculated based on the subtracted time-frequency power at their tagged frequencies respectively.

Other DDM parameters, including the response boundary, starting point, and non-decisional errors were not systematically manipulated under the present experimental design, and therefore were not subject to the analysis. While factors such as the individual handedness and the trial sequence could have potential effects on the response tendency and decisional threshold, theoretically these effects should be counterbalanced on average, as trials in different conditions were equal in number and were presented in random orders.

It is worth addressing one potential concern about the validity of the drift rate calculation method used in the present study. Since the perceptual input value p_i was assumed to be either +1 if its direction matched with the correct response, or -1 if its direction was opposite to the answer, it led to a practical fact that drift rates in the congruent trials would always be calculated as the sum of the attention distribution of the target and the flankers in mathematical values, while the incongruent drift rates would always be calculated by subtracting the flanker attention distribution from the targets. As a result, it might seem like the drift rates were computed in two different ways depending on congruency, and testing the drift rate differences between congruencies might become a mere circular justification. However, this concern should not invalidate the drift rate analyses. By principle, the input value of each stimulus at the single-trial level was determined by its spatial or semantic properties, in our case towards the left or the right, but not by its task-related function (i.e., target or flanker) or by trial congruency. In practice, the input value of each stimulus was defined to be ±1 for two main reasons:

First, the experimental design did not allow us to effectively measure the spatial properties of the stimulus. The time-frequency difference (TFD) data recorded at the tagging frequencies was influenced only by the perceptual intensity and attention distribution of the tagged stimulus, but not by its orientation. Although theoretically such spatial properties could be derived from activity in neurons that are selectively responsive to shapes and orientations (e.g., Averbeck et al, 2003; Zylberberg et al., 2016), collecting these activities requires techniques with an extremely high resolution, such as single-cell recording. Electroencephalography (EEG) does not allow us to do so. In the absence of orientation information in the time-frequency signal, I had to manually assign a perceptual input value to each stimulus based on the known information.

Secondly, I merged the left- and right-response trials when analyzing the effects between congruency and flicker conditions. Like most studies on the flanker effect, I assumed trials with left- and right-responses had no systematic difference in their cognitive and neural mechanisms of decisions, and combining these trials together would make the analysis more likely to be generalised. For these merged conditions, the absolute spatial orientation of a stimulus became no longer important, and an alternative source of input value based on relative measurements was needed. As a result, I uniformly defined a standard absolute value of 1 to each stimulus and assign it to be positive or negative relative to the orientation of the trial correct answer. The input value of a stimulus in the correct orientation would be positive, whereas those in the incorrect orientation would be assigned as negative. Conceptually, such assignments were completely driven by the inherent properties of the stimulus. Even though these values could also be used to reflect the trial congruency when the whole stimulus set was

evaluated, by principle they are still independent from the congruency per se. This point was also addressed in the work from White et al. (2011). Therefore, comparing the drift rates between congruencies was considered as not a subject to a circular justification problem.

3. Results

3.1. Behavioural Results.

I recorded behavioural response time (RT) in milliseconds and accuracy (ACC; proportion of correct responses) for all participants in all conditions. Mean ACC and RT for each condition are presented in Table 1 and illustrated in Figure 5. I conducted a 2 (Congruency: congruent vs. incongruent) × 3 (Flicker: 24Hz target/18Hz flanker vs. Static target/Static flanker vs. 18Hz target/24Hz flanker) repeated-measures ANOVA, which revealed significant main effects of congruency ($F(1, 27) = 210.575$, $p < .001$, $\eta_p^2 = .479$) and flicker ($F(2, 54) = 6.991$, $p < .01$, $\eta_p^2 = .206$) on RT. Significant congruency ($F(1, 27) = 24.845$, $p < .001$, $\eta_p^2 = .479$) and flicker ($F(2, 54) = 3.563$, $p < .05$, $\eta_p^2 = .117$) main effects were also found on ACC. No congruency × flicker interaction was found on neither RT nor ACC.

Overall, the results replicated the standard flanker effect. Post hoc pairwise comparisons corrected by Tukey's HSD tests suggested that incongruent condition exhibited significantly slower responses (MD = - 34.234, SE = 2.359, $t(27) = -14.511$, $p < .001$) and lower accuracies (MD = .032, SE = .006, $t(27) = 4.985$, $p < .001$) than the congruent. Flicker condition C (18Hz target/24Hz flanker) tended to have slightly but significantly longer RT (MD = 6.348, SE = 1.702, $t(54) = 3.730$, $p < .001$) than condition B (Static target/Static flanker). ACC in condition C was also significantly (albeit trivially) lower than condition A (24Hz target/18Hz flanker) (MD = -.007, SE = .003, $t(54) = -2.430$, $p < .05$) and B (MD = -.006, SE = .003, $t(54) = -2.172$, $p = .085$). Detailed ANOVA and pairwise contrast results are presented in Table 3 and 4 in Appendix A.

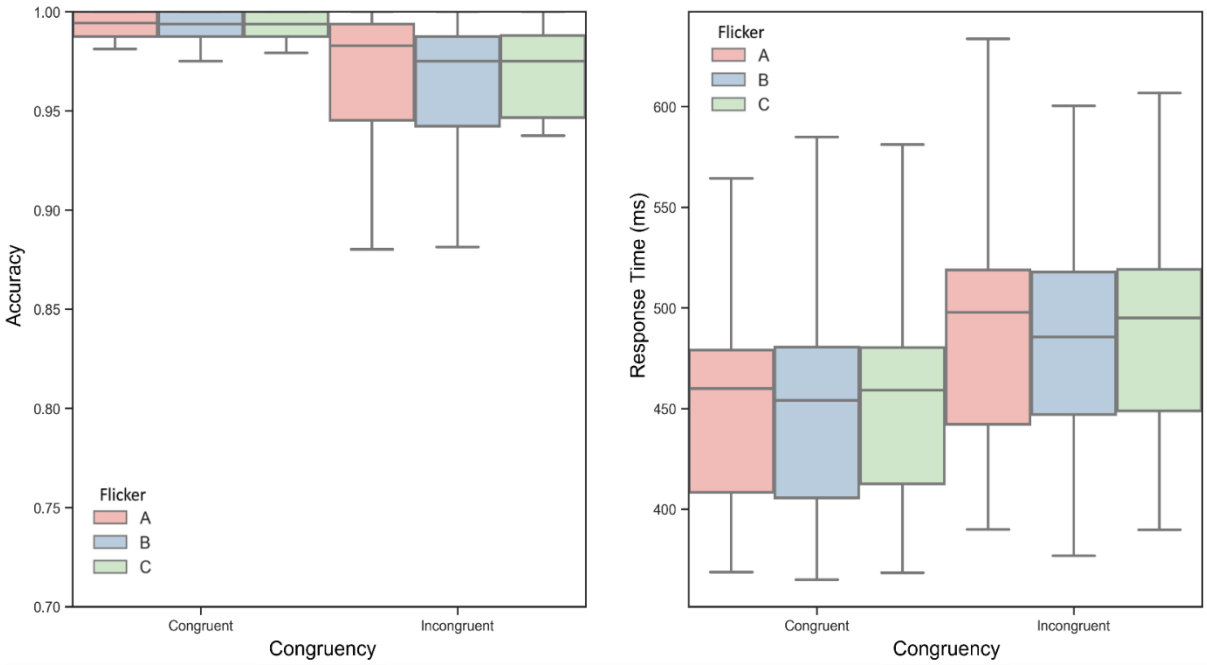

Figure 5. Boxplots showing the group means and distributions of behavioural response accuracy (left panel) and response time (right panel) in milliseconds in each congruency × flicker condition. Flicker condition A (24Hz target/18Hz flanker) was presented in red, B (Static target/Static flanker) in blue, and C (18Hz target/24Hz flanker) in green.

Table 1.
Detailed group means and standard deviations of behavioural response accuracy and response time in each congruency × flicker condition.

Condition	Accuracy		Response Time (ms)	
	Mean	*SD*	Mean	*SD*
ACO	.993	.008	465.975	73.998
AIN	.961	.043	501.633	78.182
BCO	.991	.013	464.515	73.557
BIN	.962	.033	495.983	74.989
CCO	.987	.020	468.810	76.847
CIN	.953	.052	504.385	74.241

Note. SD = Standard deviation. Conditions were named as the combination of its assigned flickers (A = 24Hz target/18Hz flanker; B = Static target/Static flanker; C = 18Hz target/24Hz flanker) and congruency (CO = Congruent; IN = Incongruent).

3.2. Lateralized Readiness Potential.

Stimulus-locked event-related potentials (ERPs) recorded from C3' and C4' were classified as contralateral or ipsilateral to the correct response hand in each condition. The ipsilateral waveforms were then subtracted from the contralateral ones to calculate the lateralized readiness potentials (LRPs). Figure 6 illustrates the LRP waveforms in each condition. Based on the literature (e.g., Gratton et al., 1988; Kappenman et al., 2021) and the overall patterns of the present data, the LRP analyses in the present study focused on the negative deflection in the subtracted waveform between 150 and 450 ms time window post-stimulus. To better understand the role of LRP in the decision-making process, the LRP component was examined not only by the mean amplitude (LRP Amplitude) over the defined time window, but also by the peak latencies of LRPs (LRP Latency). The peak latency was defined as the time point at which the LRP amplitude reached its maximum.

2 × 3 repeated-measure ANOVA tests were applied to LRP Amplitude and LRP Latency. A significant flicker × congruency interaction was found on LRP Amplitude ($F(2, 54) = 3.909$, $p < .05$, $\eta_p^2 = .126$). Pairwise comparisons (Tukey's HSD corrected) showed that condition AIN (24T/18F-Incongruent) resulted in significantly larger mean amplitude (MD = -.113, SE = .040, $t(107) = -2.801$, $p < .05$) than condition CIN (18T/24F-Incongruent). No significant congruency or flicker main effect was found in LRP Amplitudes. For LRP Latency, I observed a significant congruency main effect ($F(1, 27) = 30.730$, $p < .001$, $\eta_p^2 = .532$), suggesting that LRP reached to its peak significantly faster in the congruent condition than the incongruent (MD = -56.271, SE = 10.205, $t(27) = -5.543$, $p < .001$). No significant flicker effect was observed in LRP

Latency. Full ANOVA and pairwise comparison statistics for LRP Amplitude and LRP Latency are presented in Table 5 and Table 6 in Appendix B.

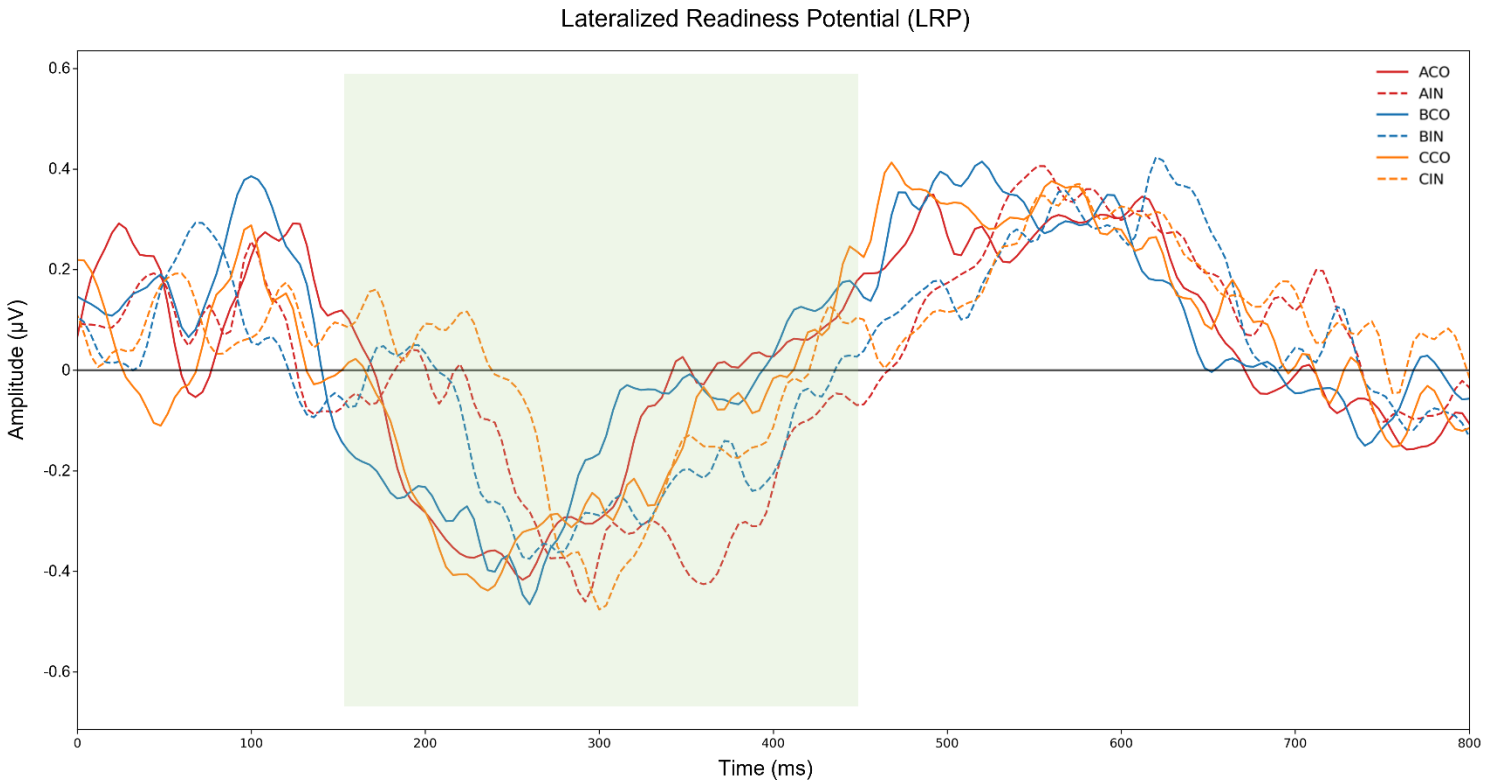

Figure 6. Grand average lateralized readiness potential (LRP) amplitudes as a function of time. LRP analyses in the present study focused on the main component of LRP in the time window (150 - 450 ms) highlighted in green. Solid lines represented the congruent (CO) conditions, and dashed lines represented the incongruent (IN) conditions. Red, blue, and orange lines represented the flicker condition A (24Hz target/18Hz flanker), B (Static target/Static flanker), and C (18Hz target/24Hz flanker), respectively.

3.3. Event-Related Potentials (ERPs).

Figures 7, 8, and 9 show the stimulus-locked event-related potentials (ERPs) recorded at the Oz (midline occipital), Pz (midline parietal), and CPz (midline central-parietal) sites, respectively. At each site, 3 major ERP components were identified for analysis, namely N1, P2, and P3. N1 was defined as the negative deflection occurring approximately 100-150 ms post-stimulus. P2 and P3 were the positive waveforms occurring between 150-250 ms and 250-450 ms, respectively. Each ERP component was measured by the mean amplitude (Amplitude) in μV in its defined window. For P3, the aspects of peak latency (Latency), peak amplitude (Maximum), and component duration (Duration) were additionally measured to better characterise the results after visually inspecting the ERP waveforms. The peak of a component was defined as the time point at which its amplitude reached the maximum absolute value, while the component duration was defined as the interval where the waveform exceeded 1/3 of its peak amplitude (Picton et al., 2000). For ease of description in the following sections, each ERP measure is named as the combination of the component, the recording electrode, and the specific aspect of ERP. For example, the mean amplitude of N1 recorded in Oz would be labelled as "$N1_{Oz}$ Amplitude".

2 × 3 repeated-measure ANOVA tests were applied to each ERP measure at each site. The complete ANOVA and pairwise contrast statistics are presented in Table 7 - 12 in Appendix C. Significant flicker main effects were found in the mean amplitudes of N1 components at Oz ($F(2, 54) = 41.810$, $p < .001$, $\eta_p^2 = .608$), Pz ($F(2, 54) = 22.430$, $p < .001$, $\eta_p^2 = .454$), and CPz ($F(2, 54) = 24.620$, $p < .001$, $\eta_p^2 = .477$). Pairwise comparisons (Tukey's HSD corrected) showed that condition B obtained significantly

stronger N1 than condition A (Oz: MD = -.832, SE = .112, $t(27) = -7.414$, $p < .001$; Pz: MD = -.377, SE = .076, $t(27) = -5.001$, $p < .001$; CPz: MD = -.199, SE = .004, $t(27) = -5.552$, $p < .001$) and condition C (Oz: MD = -.832, SE = .112, $t(27) = -7.414$, $p < .001$; Pz: MD = -.377, SE = .076, $t(27) = -5.001$, $p < .001$; CPz: MD = -.199, SE = .004, $t(27) = -5.552$, $p < .001$). No other congruency main effect or flicker × congruency interaction was observed in N1 mean amplitudes.

Similarly, significant flicker main effects were also observed in the mean amplitudes of the P2 components at Oz ($F(2, 54) = 10.980$, $p < .001$, $\eta_p^2 = .289$), Pz ($F(2, 54) = 18.360$, $p < .001$, $\eta_p^2 = .405$), and CPz ($F(2, 54) = 4.044$, $p < .05$, $\eta_p^2 = .130$), and pairwise comparisons revealed significantly stronger P2 in condition B than in condition A (Oz: MD = .339, SE = .079, $t(27) = 4.277$, $p < .001$; Pz: MD = .326, SE = .062, $t(27) = 5.262$, $p < .001$; CPz: MD = .077, SE = .034, $t(27) = 2.273$, $p = .07$) and C (Oz: MD = .301, SE = .079, $t(27) = 3.799$, $p < .01$; Pz: MD = .324, SE = .062, $t(27) = 5.233$, $p < .001$; CPz: MD = .089, SE = .034, $t(27) = 2.617$, $p < .05$). Again, no congruency main effect or flicker × congruency interaction was observed on P2 mean amplitudes in none of the channels.

For the P3 component at the Oz electrode, there was a near-significant main effect of congruency in the mean amplitude measure ($F(1, 27) = 3.760$, $p = .063$, $\eta_p^2 = .122$), revealing weaker P3 amplitude in the congruent condition than in the incongruent (MD = -.110, SE = .057, $t(27) = -1.939$, $p = .063$). No other meaningful main effect or interaction was found in the peak latency, peak amplitude, or the duration measure at Oz. At site Pz, on the other hand, P3 exhibited a significant congruency main effect in peak latency ($F(1, 27) = 7.814$, $p < .01$, $\eta_p^2 = .224$), peak amplitude ($F(1, 27) = 10.740$, p

< .01, η_p^2 = .285), and component duration (F(1, 27) = 14.620, p < .001, η_p^2 = .351); but no notable main effect or interaction was found in the mean amplitude of P3. Post hoc comparisons showed advanced peak latency (MD = -12.0, SE = 4.310, t(27) = -2.795, p < .01), enhanced peak amplitude (MD = .222, SE = .068, t(27) = 3.277, p < .01), and shortened duration (MD = -12.3, SE = 3.210, t(27) = -3.823, p < .001) in the congruent conditions than the incongruent. A similar pattern was also observed for P3 at CPz, but only the peak amplitude measure showed a significant congruency main effect (F(1, 27) = 4.703, p < .05, η_p^2 = .148), reflecting slightly stronger maximal amplitude in the congruent conditions than the incongruent ones (MD = .08, SE = .037, t(27) = 2.169, p < .05).

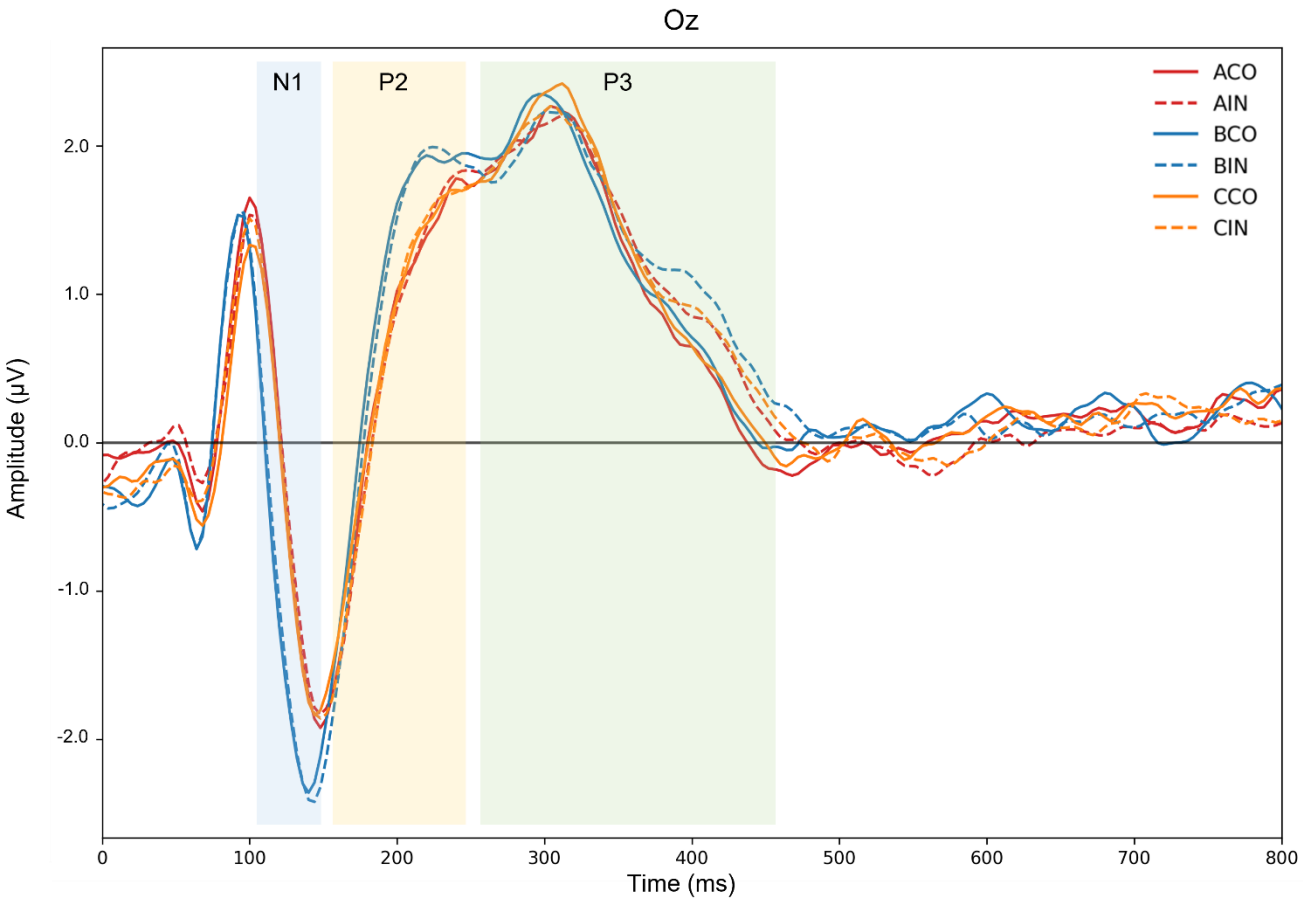

Figure 7. Grand average event-related potential (ERP) amplitudes collected at electrode Oz as a function of time. Time windows of N1 (100 - 150 ms), P2 (150 - 250 ms), and P3 (250 - 450 ms) components were highlighted in light blue, light yellow, and light green, respectively. Solid lines represented the congruent (CO) conditions, and dashed lines represented the incongruent (IN) conditions. Red, blue, and orange lines represented the flicker condition A (24Hz target/18Hz flanker), B (Static target/Static flanker), and C (18Hz target/24Hz flanker), respectively.

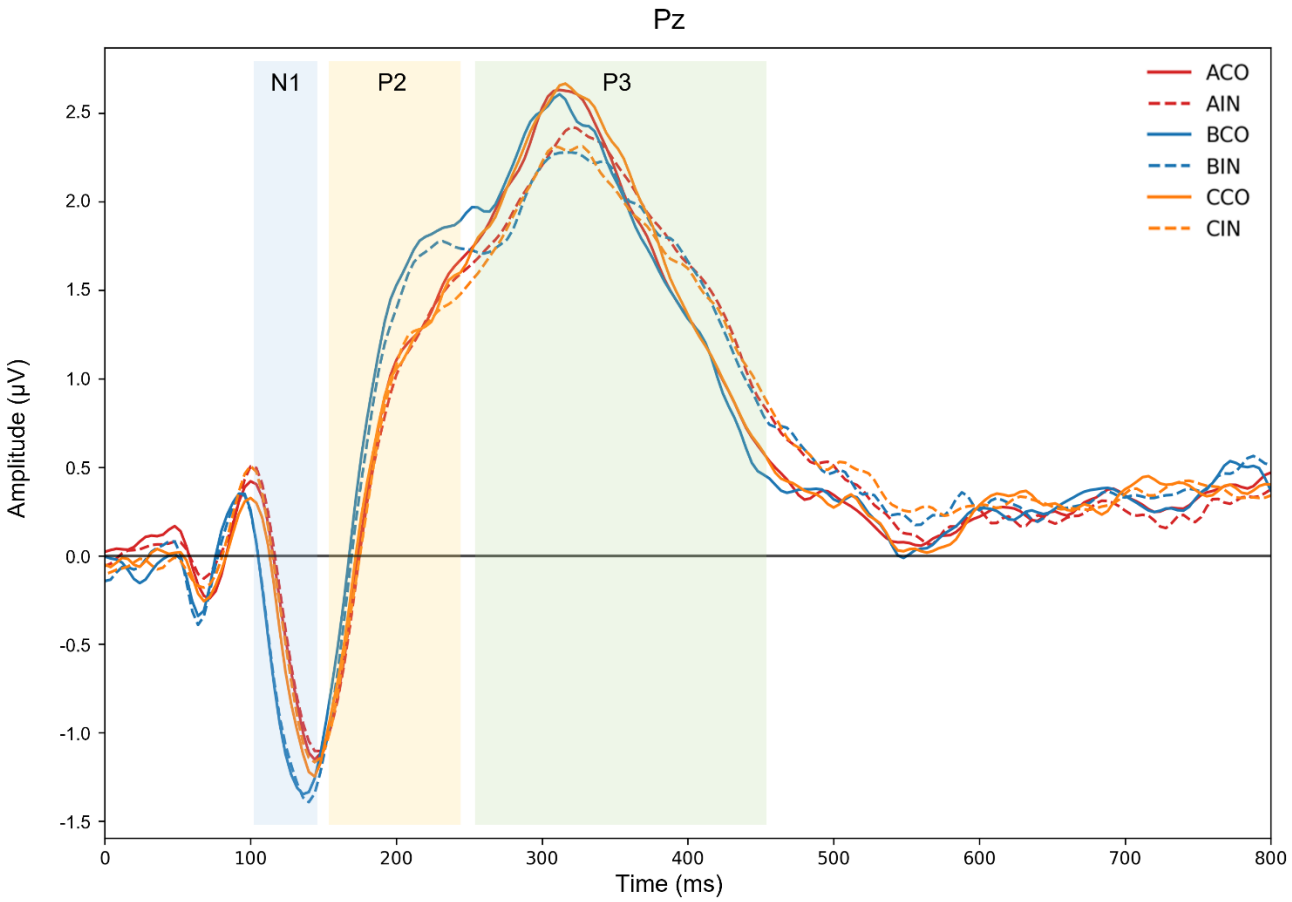

Figure 8. Grand average event-related potential (ERP) amplitudes collected at electrode Pz as a function of time. Time windows of N1 (100 - 150 ms), P2 (150 - 250 ms), and P3 (250 - 450 ms) components were highlighted in light blue, light yellow, and light green, respectively. Solid lines represented the congruent (CO) conditions, and dashed lines represented the incongruent (IN) conditions. Red, blue, and orange lines represented the flicker condition A (24Hz target/18Hz flanker), B (Static target/Static flanker), and C (18Hz target/24Hz flanker), respectively.

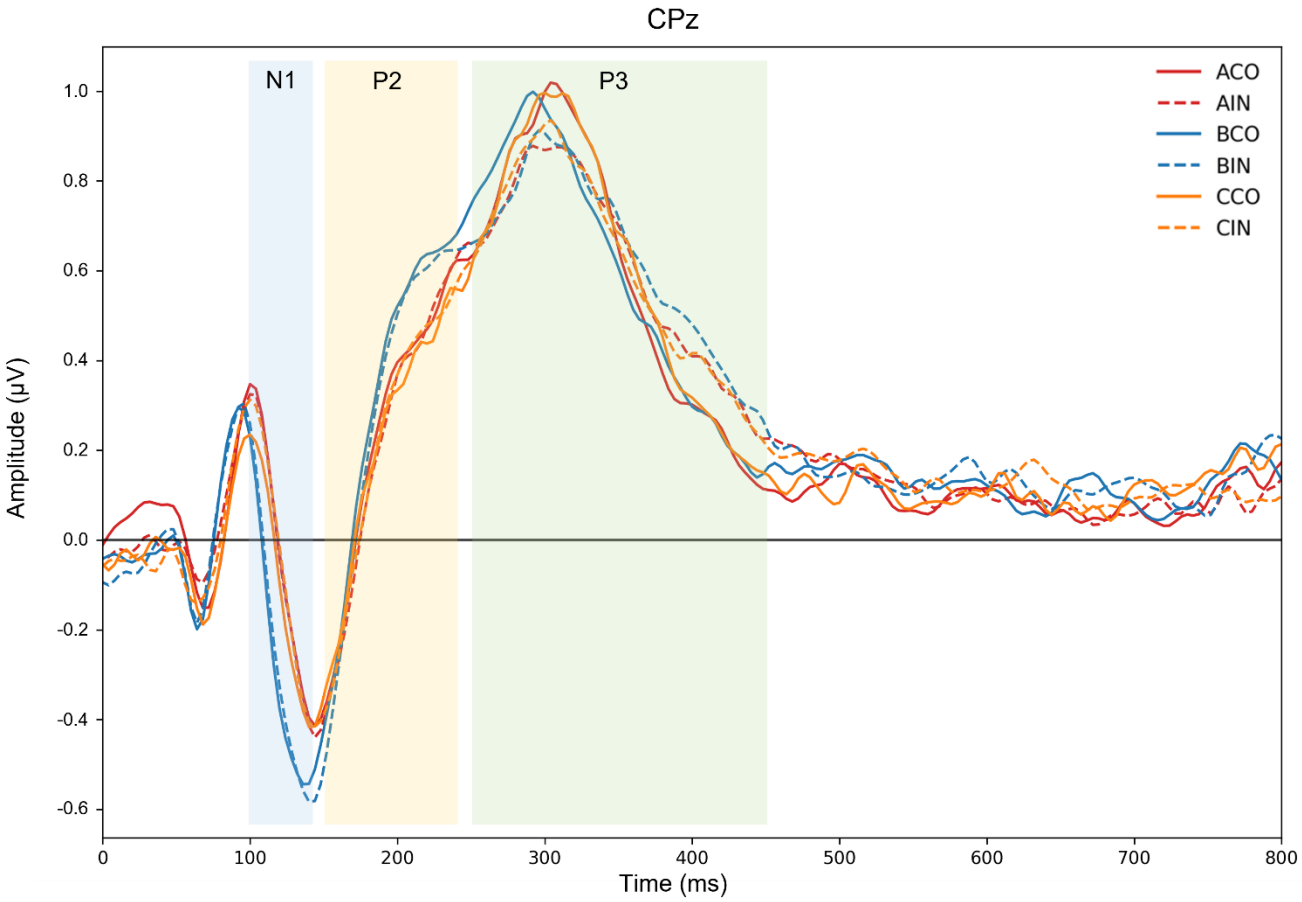

Figure 9. Grand average event-related potential (ERP) amplitudes collected at electrode CPz as a function of time. Time windows of N1 (100 - 150 ms), P2 (150 - 250 ms), and P3 (250 - 450 ms) components were highlighted in light blue, light yellow, and light green, respectively. Solid lines represented the congruent (CO) conditions, and dashed lines represented the incongruent (IN) conditions. Red, blue, and orange lines represented the flicker condition A (24Hz target/18Hz flanker), B (Static target/Static flanker), and C (18Hz target/24Hz flanker), respectively.

3.4. Time-Frequency Data.

Similar to the ERP results, time-frequency analyses were applied to the EEG data from 3 major electrodes (Oz, Pz, CPz). Figure 10 illustrates the time-frequency representations in each condition recorded at each of the electrodes. The time-frequency data from the stimulus-flashing conditions (ACO/AIN/CCO/CIN) were then subtracted by corresponding stimulus-static (BCO/BIN) conditions at each electrode to calculate the amount changed from the non-flashing baselines, here termed "time-frequency differences" (TFDs). The subtracted TFDs were examined between 0 and 500 ms post-stimulus. The boundary of this time window was determined by the average behavioural response time. To inspect whether the data reflected reliable enhancements from the baselines, TFDs were split into 5 100-ms-long bins. Figure 11 shows the representations of TFDs calculated at each flashing condition at each electrode.

One-sample t-tests were applied to the mean TFD over each bin at each stimulus-tagging (i.e., the target or the flanker) frequency at each site for each condition. These examination results would be evaluated overall and allow us to distinguish the sites and time windows that TFDs could be credibly used for further stage analyses. In general, TFDs were reliably found at Oz, Pz, and CPz. The initial 0-100 ms bin showed almost no significant TFD at any of the sites and conditions, and at neither the target nor the flanker frequency. However, all subsequent bins (100-200 ms, 200-300 ms, 300-400 ms, 400-500 ms) at all 3 sites exhibited significantly positive TFDs at both the target- and the flanker-tagged frequencies in most of the conditions, indicating that TFDs observed during these periods could reliably reflect the influence of the stimuli flashing on the corresponding rates. The detailed t-test results are presented in Tables 13 - 18 in Appendix D. According to these results, the next-step drift rate analyses will be limited within the time range between 100 and 500 ms post-stimulus.

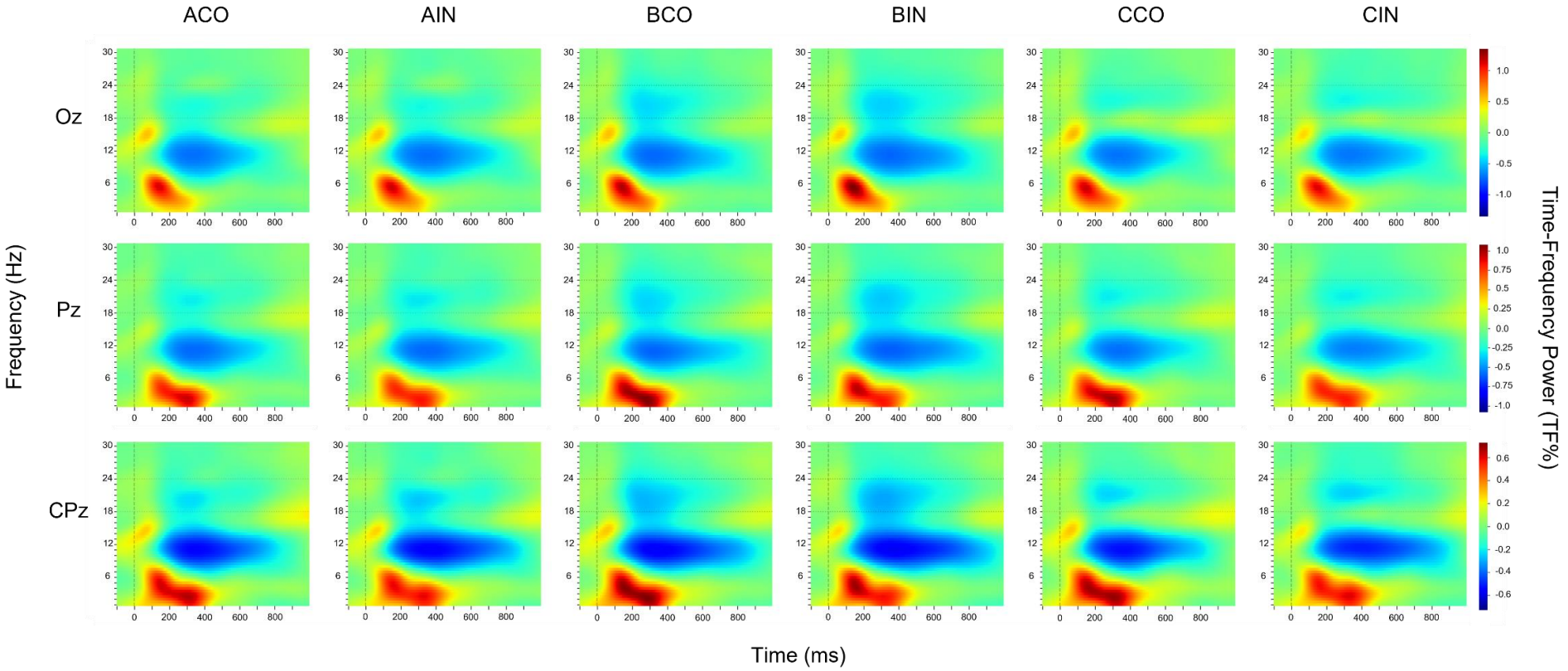

Figure 10. Time-frequency representation collected at electrode Oz (top), Pz (middle), and CPz (bottom) in each congruency × flicker conditions. Conditions were named as the combination of its assigned flickers (A = 24Hz target/18Hz flanker; B = Static target/Static flanker; C = 18Hz target/24Hz flanker) and congruency (CO = Congruent; IN = Incongruent). Time-frequency power were corrected as the percentage changed (TF%) relative to the baseline (-600 - -100 ms).

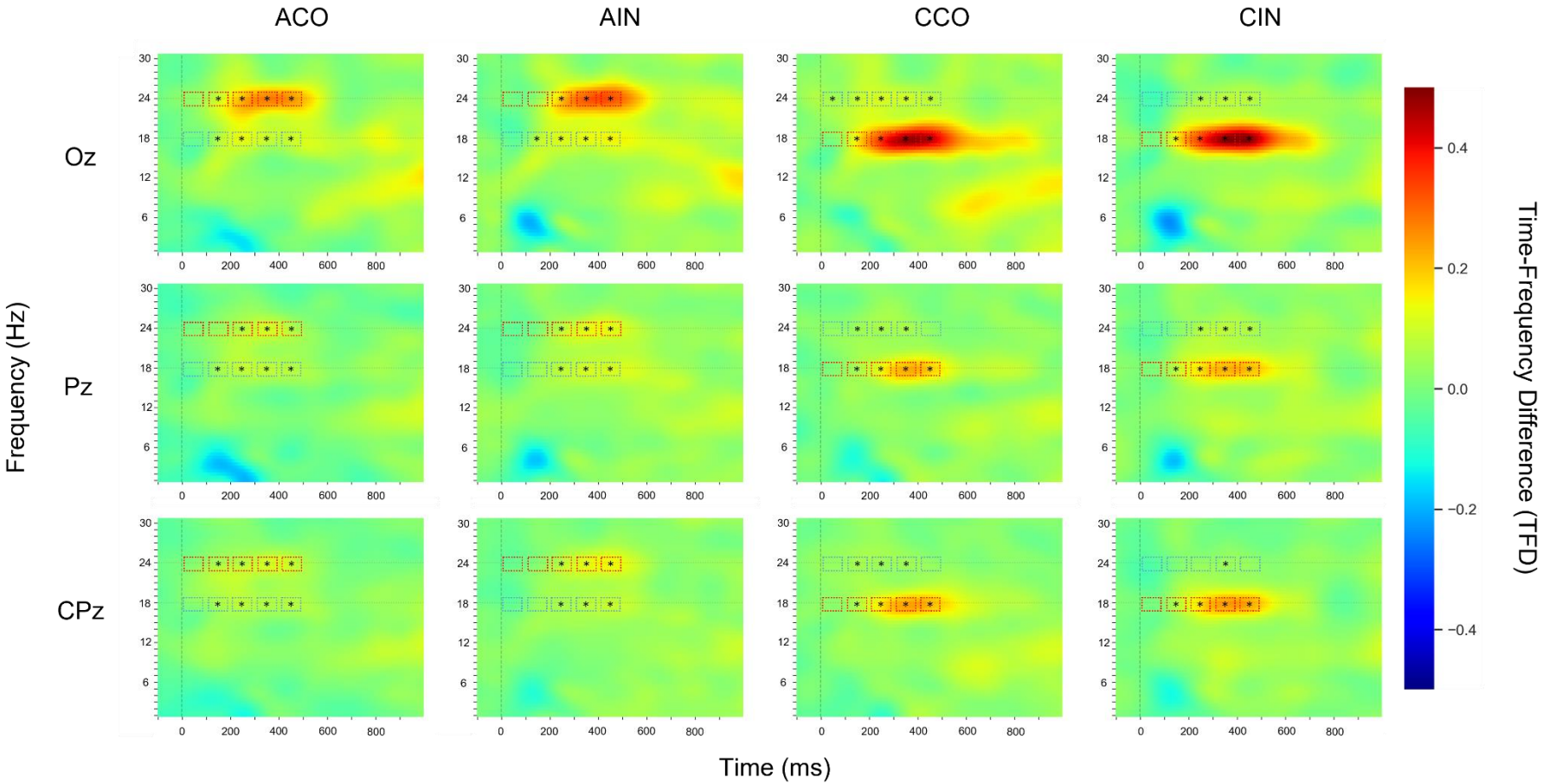

Figure 11. Time-frequency difference (TFD) representations at electrode Oz (top), Pz (middle), and CPz (bottom) in each congruency × flicker conditions. Conditions were named as the combination of its assigned flickers (A = 24Hz target/18Hz flanker; C = 18Hz target/24Hz flanker) and congruency (CO = Congruent; IN = Incongruent). For each condition at each electrode, TFDs between 0 and 500 ms were evenly divided into 5 100-ms-long time bins, and t-tests were applied to the mean TFDs in each time bin at the target-tagging (red) and the flanker-tagging (blue) frequencies. * $p < .05$.

3.5. Drift Rate.

Based on the overall evaluations on the time-frequency difference (TFD) results, the drift rate (v) analyses concentrated on the interval between 100 and 500 ms post-stimulus at Oz, Pz, and CPz. Considering the common understanding that the evidence accumulation is a continuous process with a duration shorter than the overt response time, calculating the drift rates separately at each 100-ms-long time window would probably be overly discrete and lead to difficulties in showing the whole picture, while counting the overall period between 100 and 500 ms would be too general and might include irrelevant noises into account. As a compromise solution, the 100-500 ms interval was evenly divided into an early (100-300 ms) and a late (300-500 ms) time window, each being 200-ms in duration. Mean drift rates were calculated for each window using the corresponding TFD data based on the formula adapted from White et al. (2011). Similar to the ERP components in the previous sections, each drift rate measure was named after the combination of its corresponding electrode and time stage. For example, the mean drift rate calculated in Oz at the early window would be labelled as "$v_{\text{Oz - early}}$". Figure 12 shows the mean drift rate in each flashing condition at each window computed at each electrode.

2 × 2 repeated-measure ANOVA tests were applied to the averaged drift rates in the early and the late stages. In the early stage, a significant main effect of congruency was observed at all sites (Oz: $F(1, 27) = 34.001$, $p < .001$, $\eta_p^2 = .557$; Pz: $F(1, 27) = 8.437$, $p < .01$, $\eta_p^2 = .238$; CPz: $F(1, 27) = 10.968$, $p < .01$, $\eta_p^2 = .289$), indicating higher drift rates in the congruent conditions than the incongruent ones (Oz: MD = .176, $SE = .030$, $t(27) = 5.831$, $p < .001$; Pz: MD = .095, $SE = .033$, $t(27) = 2.905$, $p < .01$; CPz:

MD = .091, *SE* = .027, *t*(27) = 3.312, *p* < .01). There was also a main effect of flicker condition on drift ratet (Oz: *F*(1, 27) = 14.400, *p* < .001, η_p^2 = .348; Pz: *F*(1, 27) = 6.168, *p* < .05, η_p^2 = .186; CPz: *F*(1, 27) = 9.236, *p* < .01, η_p^2 = .255), revealing lower drift rates in conditions with 24T/18F flickers than the 18T/24F ones (Oz: MD = -.147, *SE* = .039, *t*(27) = -3.795, *p* < .001; Pz: MD = -.067, *SE* = .027, *t*(27) = -2.484, *p* < .05; CPz: MD = -.065, *SE* = .022, *t*(27) = -3.039, *p* < .01). No significant interaction was found at any of the sites. Similar results were obtained at the late stage. The significant congruency main effect observed at the three sites (Oz: *F*(1, 27) = 17.390, *p* < .001, η_p^2 = .392; Pz: *F*(1, 27) = 10.256, *p* < .01, η_p^2 = .275; CPz: *F*(1, 27) = 7.146, *p* < .05, η_p^2 = .209) suggested that congruent conditions were higher in drift rates than the incongruent ones (Oz: MD = .161, *SE* = .037, *t*(27) = 4.170, *p* < .001; Pz: MD = .124, *SE* = .039, *t*(27) = 3.203, *p* < .01; CPz: MD = .084, *SE* = .031, *t*(27) = 2.673, *p* < .01). The flicker main effect was also significant (Oz: *F*(1, 27) = 8.735, *p* < .01, η_p^2 = .244; Pz: *F*(1, 27) = 6.771, *p* < .05, η_p^2 = .200; CPz: *F*(1, 27) = 8.751, *p* < .01, η_p^2 = .245), showing lower drift rates in conditions with 24T/18F flickers than the 18T/24F conditions (Oz: MD = -.203, *SE* = .069, *t*(27) = -2.956, *p* < .01; Pz: MD = -.097, *SE* = .037, *t*(27) = -2.602, *p* < .05; CPz: MD = -.113, *SE* = .038, *t*(27) = -2.958, *p* < .01). Again, no significant interaction was observed. The complete ANOVA and pairwise contrast statistics are presented in Table 19 -24 in Appendix E.

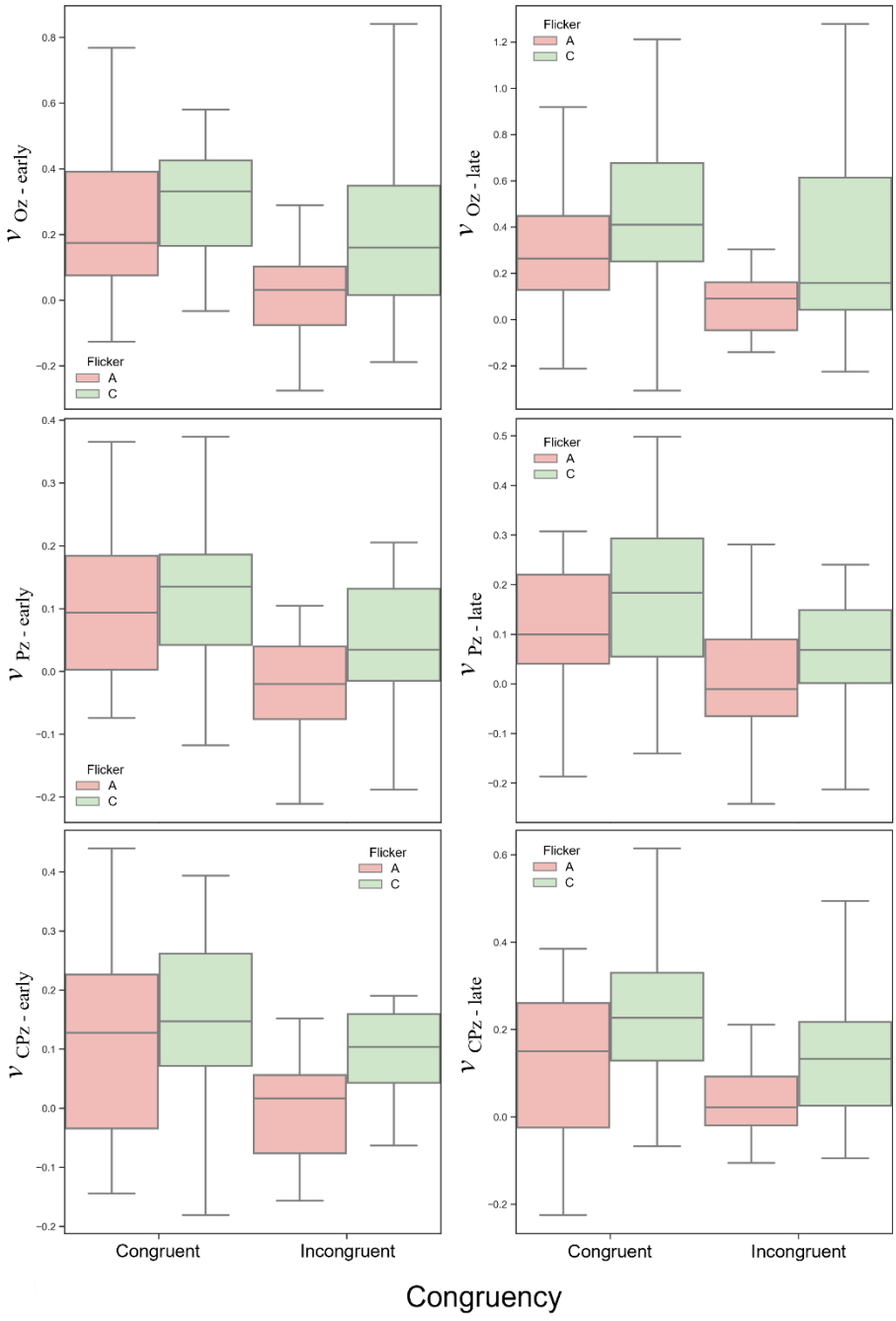

Figure 12. Boxplots showing the group means and distributions of the mean drift rates in the early (left panel) and late (right panel) stages in each congruency × flicker condition calculated at electrode Oz (top), Pz (middle), and CPz (bottom). Flicker condition A (24Hz target/18Hz flanker) was presented in red, and C (18Hz target/24Hz flanker) in green.

3.6. Correlations.

Since the ultimate goal of the present research is to find out which neural signature(s) provide the best explanation for the flanker effect, it is important to understand not only the effects of congruency on these signatures, but also their potential predictive power for the behavioural results. For this reason, I computed the correlations with RT for each measurement that showed significant variance between conditions. Non-flashing conditions (BCO/BIN) were excluded from the correlation analyses due to the lack of meaningful drift rate data. Among these measurements, RT showed significant or near-significant positive correlations with LRP Latency (r = .375, p < .001) and $P3_{Pz}$ Latency (r = .183, p = .053); whereas significant negative correlations were found with $v_{Oz\text{ - early}}$ (r = -.201, p < .05) and $P3_{Pz}$ Maximum (r = -.196, p < .05). Figure 13 presents the correlations between RT and these measures. The complete correlation statistics are shown in Table 2.

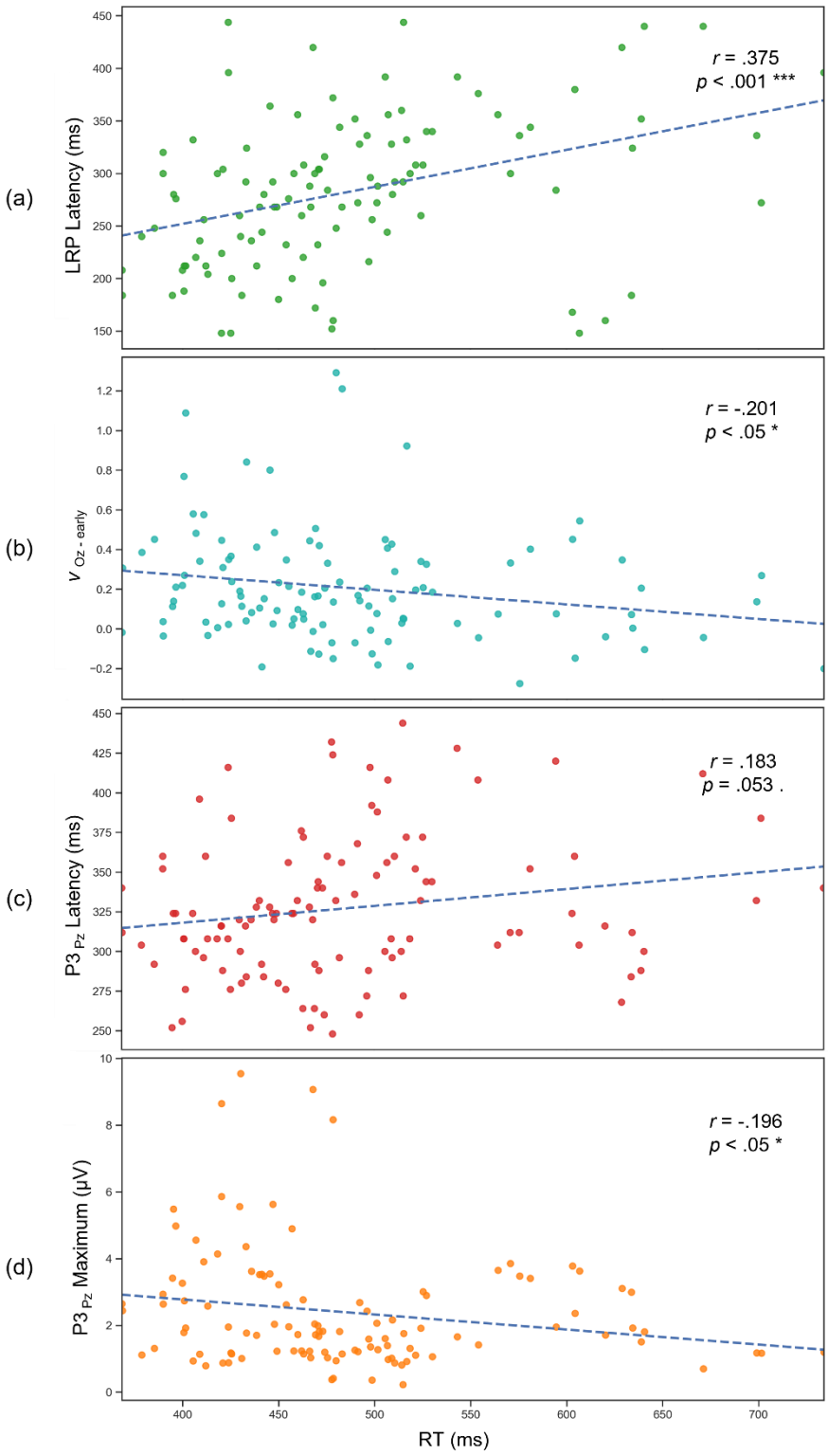

Figure 13. Scatter plots with regression lines (blue dashed) illustrating the correlations between behavioural response time (RT) and LRP latency (panel a), $v_{Oz\text{ - early}}$ (panel b), $P3_{Pz}$ Latency (panel c), and $P3_{Pz}$ Maximum (panel d). Correlation coefficients (r) and correlation significance p-values were labelled. . $p < .1$, * $p < .05$, ** $p < .01$; *** $p < .001$.

Table 2.
Correlation statistics between behavioural response time (RT) and measures revealed significant main effects or interactions in the previous ANOVA tests.

Measure	*r*	*p*
LRP Amplitude	.108	.256
LRP Latency	.375	<.001 ***
$N1_{Oz}$ Amplitude	.085	.372
$P2_{Oz}$ Amplitude	-.039	.683
$P3_{Oz}$ Amplitude	.074	.439
$v_{Oz\text{ - early}}$	-.201	<.05 *
$v_{Oz\text{ - late}}$	-.082	.390
$N1_{Pz}$ Amplitude	.074	.439
$P2_{Pz}$ Amplitude	.059	.539
$P3_{Pz}$ Latency	.183	.053 .
$P3_{Pz}$ Maximum	-.196	<.05 *
$P3_{Pz}$ Duration	.128	.179
$v_{Pz\text{ - early}}$	-.078	.413
$v_{Pz\text{ - late}}$	-.060	.531
$N1_{CPz}$ Amplitude	-.037	.697
$P2_{CPz}$ Amplitude	-.010	.919
$P3_{CPz}$ Maximum	-.084	.381
$v_{CPz\text{ - early}}$	-.146	.124
$v_{CPz\text{ - late}}$	-.061	.523

Note. r = Pearson's r-value. . $p < .1$, * $p < .05$, ** $p < .01$; *** $p < .001$.

4. Discussion

4.1. Summary of Results.

The present study examined two models of Eriksen's flanker effect, the continuous-flow model (CFM) and the drift-diffusion model (DDM). Overall, response time (RT) was shorter, and response accuracy (ACC) higher in the target-flanker congruent (CO) conditions than in the incongruent (IN) conditions. This result replicated the pattern of a typical flanker congruency effect, showing that the introduction of flashing stimulus pairs did not affect the fundamental mechanisms underlying the flanker effect. On the other hand, RTs in flicker condition A (24Hz target/18Hz flanker) tended to be longer those than in flicker condition B (Static target/Static flanker), while ACC in condition A tended to be lower than in conditions B and C (18Hz target/24Hz flanker). These variations suggested that differences in flicker pairs might also have some unexpected effects on the behavioural performances.

The lateralized readiness potential (LRP) did not show notable difference in amplitudes between conditions, except that a slightly stronger LRP was found in condition AIN than in CIN. The "Gratton dip" component was not observed in the incongruent LRP waveforms in this study. The peak latency measure revealed that LRPs in the congruent condition reached their maxima faster than in the incongruent ones, suggesting delayed motor readiness in the incongruent condition. For other event-related potential (ERP) components, N1 and P2 recorded at Oz, Pz, and CPz sites all showed stronger amplitudes in the static conditions than both of the flashing ones. The mean amplitudes of P3 were slightly stronger in the incongruent condition at the Oz site. At Pz,

the P3 component exhibited shorter peak latency, stronger peak amplitude, and shorter duration in the congruent condition than the incongruent, but no significant difference between congruencies in the mean amplitude was found. P3 at CPz showed a similar pattern as at the Pz site, though only in the peak amplitude measure showed a statistically significant between-congruency difference.

The cortical processing of the target and the flankers was examined by quantifying time-frequency power differences (TFDs) between the flashing and static conditions. At Oz, Pz, and CPz, TFDs at both the target- and flanker-tagging frequencies were reliably detected between 100 and 500 ms post-stimulus. Drift rates in each condition were calculated based on the TFDs at Oz, Pz, and CPz at an early (100-300 ms) and a late stage (300-500 ms). Results showed that the drift rates at all three sites scored higher in the congruent conditions than in the incongruent conditions in both stages. Also, flicker condition A tended to produce lower drift rates than condition C conditions at all these sites.

Finally, examining the correlations between RT and the major measures found with systematic differences between conditions, LRP peak latency showed moderately positive correlation with RT. P3 peak latency at Pz also showed weakly positive correlations with RT. The early-stage drift rate at Oz and the peak amplitude of P3 at Pz showed weak negative correlation with RT. No other measure was found to have significant correlation with RT.

4.2. LRP, the Continuous-Flow Model, and the "Gratton Dip".

The continuous-flow model was not supported by the results from the present study. For the continuous-flow model (CFM), the primary neural measure examined in the present study was the lateralized readiness potential (LRP), and observing the "Gratton dip" component in the LRP waveforms was of particular interest. As a reminder, the "Gratton dip" was characterised by a slight positivity in the LRP waveform in the incongruent conditions at an early stage post-stimulus (Gratton et al., 1988; 1992). The positive "dip" was interpreted as a cortical activation favouring the wrong response. In consequence, the overall LRP amplitude in the incongruent conditions should be lower than the congruent ones if the CFM is correct.

Surprisingly, results from the present experiment did not replicate the "dip" found by Gratton et al. in 1988. The present results did not manifest any amplitude difference between congruencies on average. Although the incongruent LRPs indeed tended to be less negative than the congruent ones in the early time windows (approximately 100-300 ms), the waveforms did not go positive evidently, meaning no evidence for activation in the ipsilateral motor cortices or towards the incorrect direction. Thus, the amplitude patterns reversed later when the incongruent conditions obtained more negative LRPs than the congruent at the following stage (300-500 ms). Such reverse led to the mean amplitude equality of the overall LRP between congruencies. In contrast, the peak latency revealed significant delay in the incongruent conditions. LRPs reached their maximum slower in the incongruent trials for about 50 ms than in the congruent ones. This asynchrony also roughly matched with the RT difference between congruencies. Further,

when associating with the overt RT, LRP latency was found with a moderate positive correlation, while the LRP amplitude showed no notable correlation.

Taking these measurements together, the LRP results from the present experiment seemed to be better explained as a peak shift in LRP rather than the "Gratton dip" proposal, and the behavioural flanker effect observed in the incongruent trials was most likely due to delayed activity in the motor cortices but not weakened readiness strength or misdirected activation in the wrong response channels. In other words, the key feature influenced by the congruency in the response channels was the onset timing of readiness of the correct response but not the confusion about which response to make. In the incongruent condition, the onset of the response readiness in the primary motor cortices was lagged by the flanker interference happening at some earlier stage of the information processing, which consequently led to the extended response time as the flanker congruency effect. No consistently positive component like the "Gratton dip" from the present LRP results that could indicate any cortical preparation favouring the incorrect response hand movement was found in the incongruent condition. It further implied that the cortical readiness of motor response was more likely to be activated only once some judgement was made in the previous hierarchy, rather than being continuously influenced by the sensory inputs, in contradiction to Eriksen and Gratton's arguments in the CFM (Eriksen et al., 1985; Gratton et al., 1988) and fitted better to the prediction of the DDM. Overall, the continuous-flow model was not strongly supported by the LRP results from the present study.

4.3. The Drift-Diffusion Model.

On the other hand, the drift diffusion model (DDM) seemed to account well for the present results. The primary DDM parameter examined in the present study was the drift rate (*v*), which theoretically reflects the speed of cognitive evidence accumulation. Drift rates were calculated at Oz, Pz, and CPz based on the formula from White et al.'s work (2011). The time-frequency differences (TFDs) recorded at these sites were used to quantify the time-varying attention allocation. For the flanker effect, the diffusion model expected lower drift rates in the incongruent condition than in the congruent. DDM also predicted that drift rates should negatively correlate with the overt response time (RT) at some degree.

Our results confirmed these predictions. At all three sites, the drift rates were found significantly higher in the congruent conditions than in the incongruent at both the early (100-300 ms) and the late stage (300-500 ms). Yet, when associating with the overt RT, only the drift rate at Oz at the early stage showed a negative correlation, meaning that a faster drift rate at this site within this interval predicted a shorter response time. No drift rate result in other windows or at other sites exhibited this association with RT.

Two important facts could be revealed from these results: First, TFDs collected at the Oz site had the most explanatory power in accounting for the allocation of attention. This is consistent with the general understanding that perceptual inputs in the visual stream are retinotopically mapped onto the primary visual region and surrounding extrastriate cortices, and these projections are constantly affected by not only the bottom-up inputs but also top-down modulatory influences such as selective attention. The

retinotopic maps in the primary visual cortex are usually believed to be the lowest-level perceptual elements in the hierarchical cortical visual system, which also means they contain the most straightforward, unselected, and lossless information from perception (e.g., Crick & Koch, 1995; Hubel & Wiesel, 1962). In contrast, TFDs collected at Pz and CPz failed to well account for the time-varying attention allocation needed for the DDM calculations. The input streams could still be recognized at these regions by frequency tagging, but the retinotopic projections were more or less distorted by the functional selectivity in these higher-level extrastriate cortices (Belliveau et al., 1991; Hung et al., 2015; Turner et al., 1993). As a result, although drift rates calculated at these channels also roughly matched the congruency effect, they were unable to support reliable predictions about RTs, which undermined their explanatory power as elements of computational models. These results also indicated that the evidence accumulation process was probably dominated by some low-level mechanisms in the hierarchy of sensory processing.

Secondly, the early stage (100-300 ms post-stimulus) tended to be the critical time window for evidence accumulation. Drift rates calculated at Oz exhibited good correlation with RT only at the early but not at the late stage. This result probably means that the average time needed for making a cognitive decision in the present task was about or less than 300 ms, even though the overt responses were not yet observable at that point. This interpretation fitted a critical argument in DDM that conceptual decisions must be made before any possible response elicitations or implementations. It suggested a hierarchical relationship between the sensory and the motor systems and a threshold-like decision making mechanism. Although drift rate values could still be calculated

mathematically at the late stages since the stimulus presentations were not terminated until the responses were made, those income information at the late periods were probably less relevant to the conceptual decision making. Interestingly, this result also seemed to match the findings in the lateralized readiness potential (LRP), given that the early-stage time window's boundary at 300 ms was roughly consistent with the average peak latencies of the LRPs.

Taking these findings together, the present study supported the DDM as a computational explanation for the flanker effect, and suggests that flanker interference arises relatively early in visual processing. The successful correlation with RT indicated that drift rate could be used for not only discriminating the congruency but also providing a reliable prediction of the precise response time. These results also helped validate the feasibility of applying the diffusion model to the neurophysiological data. I have shown here that neural TFD data recorded via electroencephalography (EEG) can be integrated in the DDM framework, and the drift rates computed based on EEG enabled effective predictions about decision making and behavioural responses. Nonetheless, the correlation found between the early-stage drift rate at Oz and RT was still relatively weak, meaning its predictive power was very limited. It also indicated the potential influences from other unmodelled factors to the decisions and responses, such as the individual differences in cautiousness and decisional threshold. Considering the DDM in the present study was highly simplified, this limitation was understandable. Such factors may be able to be modelled in a comprehensive diffusion model by introducing other parameters including the starting point (z), response boundaries (a), and non-decision

errors (T_{er}). Future research may be able to quantify these parameters with some observable neural measures to improve the model.

4.4. DDM vs. CFM.

Comparing the findings from LRP and drift rate, a conclusion seems obvious: the drift-diffusion model provided a reasonable explanation for the flanker effect observed in the present study, while the continuous-flow model was not strongly supported. Responses in a standard flanker task probably involve firstly a conceptual decision and then followed by activation in the corresponding motor channels. The flanker congruency effect is mainly due to the delay in the conceptual decision process.

Overall, this interpretation is reasonable. The continuous-flow model's proposal about accumulating perceptual evidence in the response channels is probably oversimplified. Considering the efficiency of cortex utilisation, the cortical pivot of evidence accumulation is highly unlikely to locate in the lateralized primary motor cortices since it only fits decision making in the 2-alternative choice scenarios like a standard flanker task. In contrast, situations in real life are often much more complex, and most decisions people encounter could have more than two options. There are also abundant cases in which people will make internal choices without performing any overt motor responses. In some other cases, behavioural responses can be delivered by non-lateralized actions, such as the saccadic eye movements. The continuous-flow model could not well explain the decision processes in these situations, whereas the diffusion model offers a flexible framework suitable for most of them.

Nevertheless, the present result does not simply assert the continuous-flow model of the flanker effect to be false. The key problem for the continuous-flow model in the present study was the failure in replicating the classic "Gratton dip" in LRPs in the incongruent condition. Several critical differences between the present study and Gratton et al.'s works (1988; 1992) may contribute to this failure. First, the response intensities were probably stronger in Gratton et al.'s studies at the present. According to the literature, participants in these experiments made behavioural responses by squeezing dynamometers in the corresponding hands, and each response required more than 25% of the person's maximal forces to register the response. Such responses were likely to involve active uses of whole-hand and even arm muscles as well. Similar designs were also found in earlier non-EEG works that built the theoretical foundations of the continuous-flow model (e.g., Eriksen et al., 1985; Coles et al., 1985). In contrast, responses in the present experiment required only keyboard pressing with fingers, which was less effortful than dynamometer squeezing. This variation could lead to weaker motor cortex activation in participants in the present experiment when making responses, and consequently made the differences in LRPs harder to be recognized.

Second, the response strategies used in these studies might be different. Extensive studies on the speed-accuracy tradeoff have showed that people would employ strategies to control their behaviours in typical 2AFC tasks, especially when one or more aspects of their performance were highlighted or motivated (e.g., Dambacher & Hübner, 2013; Osman et al, 2000; Sanders & Lamers, 2002; Wylie et al., 2009). In Gratton's experiments, participants were explicitly instructed to emphasise their response speed over accuracies. The overt responses in Gratton's studies were often fairly quick, while

the error rates were relatively high. In one experiment (Gratton et al., 1992), for example, the average RTs for the congruent and incongruent conditions were 316 and 364 ms respectively, while the error rates were .067 for the congruent conditions and .272 for the incongruent conditions. In contrast, participants in the present experiment were not given any instruction about the speed or accuracy so that they could respond in a neutral state. The average RTs obtained in the present study were 466 ms for the congruent conditions and 501 ms for the incongruent ones, while the error rates were less than .01 and .05, respectively.

Further to the failed replication of the "Gratton dip", one possible explanation could be that the cognitive mechanisms might vary with the changes in response strategies. In speed-driven conditions like Gratton's experiments, the continuous-flow model may be a reasonable proposal, as it could allow people to respond as quickly as possible. The primary motor cortices in such situations are likely to be highly vigilant and prepared for initiating responses as quickly as possible, and this could make them sensitive to the continuous stimulus influences. Alternatively, when a neutral or accuracy-driven strategy was employed, people are more likely to make a confident conceptual decision before generating any response preparation. In more conservative situation, one may even suppress the excitations in their response channels, intentionally or not, to guarantee the correctness of their responses. These situations are more analogous to the present experiment where the diffusion model tends to provide a better explanation. Future studies may be able to examine this hypothesis using controlled comparisons between participant groups using these two strategies.

4.5. Exploratory ERP: P3 and the Flanker Effect.

Except for the LRP and drift rates, additional analyses were conducted to explore if any other neural signatures were related to the flanker effect or provide complements to the previous discussions and arguments. Specifically, finding a reliable neural indicator of the precise time of conceptual decision making was of high interest since it could not be pinpoint from the drift rate or time-frequency difference (TFD) data directly. Based on this motivation, exploratory analyses focused on the ERPs at the 3 sensory system channels (Oz, Pz, CPz) given the high temporal resolution of ERP. While the peak latency of LRPs could also show some clues about the decision time boundary, arguably it was still not directly reflecting activities in the sensory system. According to the expectation, a valid ERP marker of cognitive decision should exhibit some peak shifts between congruencies which might indicate the delayed decision making in the incongruent conditions.

The actual results, however, were more complicated than expected. At site Oz, the mean amplitude of P3 overall was slightly higher in the incongruent conditions, but no other measurement showed notable variances between congruencies. At site Pz, the between-congruency difference was found in several aspects of the P3 components. The incongruent conditions were found with not only delayed peak latencies, but also attenuated maximal amplitudes and extended component durations. Similar pattern was also found at site CPz, though only the difference in peak amplitude reached a statistically significant threshold. Thus, the peak latency of P3 at Pz showed a weakly positive correlation to the overt RT, while the P3 maximal amplitude at Pz was weakly negatively correlated with RT. Taking these observations together, the ERP results could

be concluded as a weaker but more durable P3 at site Pz, probably also CPz, in the incongruent trials than in the congruent ones.

One way to interpret these results was that P3 at Pz/CPz indeed indicated the cognitive decision making process, and a decision was made at the time P3 reached its peak. This interpretation was mainly supported by the delayed peak latency in the incongruent trials, which suited with the previous arguments of slower cognitive decision based on drift rates and LRPs. The positive correlation between P3 latency and RT also favoured this explanation. A potential reason for this result could be that the intensities of cognitive decisions were averagely lower in the incongruent trials due to factors such as lower subjective confidence. However, few theories or empirical evidence could stand for this hypothesis, neither could it be verified with the existing data. Thus, such interpretation could not account for the attenuated peak amplitude as well as the extended duration found in the incongruent conditions. Also, the P3 at Pz and CPz tended to reach its peak after 300 ms post-stimulus on average, later than the LRP peak latencies discussed previously, meaning it occurred after the response preparation initiated in the motor channels. This contradicted with the previous argument based on DDM that cognitive decisions were made prior to the start of response readiness. In addition, disparities of P3 latency between congruencies were also relatively small in size and were not so proportional to the disparities in the overt RT or the LRP latency. Hence, the present findings at P3 probably did not indicate differences in cognitive decision making in the flanker task.

An alternative interpretation was that P3 at Pz/CPz reflected the strength of attentional control engaged in the ongoing monitoring and processing of the sensory

inputs. In the incongruent trials, the attentional control could be weakened since the attentional resource was more likely to be divided and distributed to the flankers, leading to the attenuation in P3 peak amplitudes. This explanation was consistent with findings from several works about P3 under multi-task environments, which reported weakening P3 amplitudes as more distractors were presented simultaneously (Isreal et al., 1980). Evidence from visual oddball studies also found decreases in P3 amplitudes when task difficulty increased (Kramer et al., 1985; Wickens et al., 1983). On the other hand, given the experimental design that the trial presentation would not be terminated until a behavioural response was carried out, the stimulus exposures in the incongruent trials were on average longer than in the congruent ones in the same way as the flanker effect in RT, and such prolonged exposure was likely to result in the extended P3 duration observed at these channels. This interpretation would probably be more appropriately explain the observations in P3.

4.6. Limitations.

Despite the findings discussed above, it should be addressed that the present study was a first-step attempt of bridging the cognitive theories of the flanker effect with actual neural data. Many aspects of the present experimental design and analysis methods were still relatively primitive, and several limitations must be addressed.

4.6.1. The Flicker Effect.

A major source of potential issues came from the variances between conditions with different target-flanker flicker pairs. In fact, notable main effects were found not only between congruencies but also between flicker pairs in most of the examined measurements.

One type of the variance was between the static condition (B) and the two flashing conditions (A and C). In the behavioural performance results, both conditions A and C scored longer response time (RT) than the conditions with static stimuli on average. Condition C also obtained lower accuracy (ACC) than in the static and the condition A. Similar patterns were observed from the event-related potential (ERP) results as well. At site Oz, Pz, and CPz, the mean amplitudes of the N1 and P2 components were found weaker in both of the flashing conditions in contrast to the static condition. A possible explanation to this type of variances could be the changes of perceptual intensity in the flashing conditions. In contrast to static stimuli, flickers achieved via stimulus on/offset alterations would have only half of the effective exposure within the same unit of time. Consequently, the physical intensity of input from the flashing stimuli, also known as the luminous flux, would theoretically be less than the static counterparts in a linear system and be perceived as “dimmer”. This interpretation was supported by the attenuated amplitudes in the flashing conditions in N1 and P2, since these components were known to be highly sensitive to the intensity of visual stimuli (e.g., Carrillo-De-La-Peña et al, 1999; Vogel & Luck, 2000). Importantly, this type of variance violated the assumption that introducing flashing stimuli would not cause systematic differences from the static condition other than the presence of frequency-

tagged neural markers, which could in consequence undermine the validity of using the static condition as the baseline in the subsequent time-frequency power subtractions. Nonetheless, pairwise comparisons suggested that effects of flashing stimuli on the behavioural performances were extremely limited. Overall, the RT delays in the flashing conditions were less than 5 ms, and the ACC declines were less than .01. Thus, these differences between the flashing and the static conditions did not show notable interference with the congruency effect in the flanker task, which was of the primary research interest. Therefore, this assumption violation probably would not greatly damage the major arguments about the flanker effect, but investigations on other potential influences from it can still be worthwhile for future studies.

The other type of variance occurred between the two flashing conditions with different flicker pairs. In the time-frequency difference (TFD) and drift rate results, the 18T/24F condition obtained stronger mean drift rates than the 24T/18F conditions in both time windows at Oz, Pz, and CPz. Such variance was most likely due to the disparities in the relative saliency between stimuli flashing on different rates. A well-known illusion in the studies of periodic visual stimulus was called the flicker fusion, which describes a tendency of perceiving a rapid-flashing stimulus as a near-steady one at weakened contrast (Simonsen & Brozek, 1952). This tendency increases as the flashing rate of the stimulus becoming faster until approaching to a critical threshold, sometimes known as the flicker fusion rate. This phenomenon was also extensively learned as an important factor of the visual persistence effect (Anderson & Anderson, 1993). Most researchers now believe that the flicker fusion effect is caused by the difficulty of the visual system in discerning the differences between the repetitive rapid stimulus on/offsets (Kelly,

1964; Landis, 1954). On top of the flicker fusion effect, it has been empirically testified that flickers at lower rate, in other words perceptually less steady, tend also to be more salient in perceptions. Many studies on the steady-state visual evoked potential (SSVEP) reported stronger amplitudes induced by lower frequency flickers than the rapid ones (e.g., Lee et al., 2011; Norcia et al., 2015; Pisarchik, Chholak, & Hramov, 2019). Researchers believed this was because flashier stimuli are more likely to trigger the change detection mechanisms in the human sensory system and get better discriminability from the backgrounds (e.g., Gawen & Martin, 2002; He & Lau, 2014; Hong, Thong, & Tam, 2004; Itti & Koch, 2001; Li, 2002).

In the present study, the target and flankers were simultaneously presented at two dissociable flashing rates, which probably led to variations in the perceived steadiness between the two types of stimuli, and consequently made the slow-flashing stimulus stand out from the rapid-flashing rests. Specifically, the saliency of the target relative to the flankers in the 24T/18F condition would be attenuated, while the relative saliency of the target in the 18T/24F condition would be amplified. Such saliency differences could be further intensified by modulations from selective attention mechanisms. As a result, participants were more likely to recognize and react faster to the targets in the 18T/24F condition in contrast to the 24T/18F, manifested as higher drift rates. Nonetheless, this saliency effect was most strongly found on the TFD-based drift rate results but was not evident in other measurements including the behavioural RT, the lateralized readiness potential (LRP) and other ERP components. This probably meant that the saliency differences in the present design did not impair the flanker effect at the overt response

level as much as at the sensory level. Systematic reviews in the future are needed to gain more detailed understandings on the exact effect of flicker pair manipulations.

4.6.2. Uncontrolled Drift-Diffusion Parameters.

The second major defect of the present study was the absence of effective control on the drift-diffusion model (DDM) parameters other than the drift rate. As mentioned in the introduction, a complete DDM according to Ratcliff (1978) should be able to define 4 key parameters, namely the drift rate, the decisional boundary, the starting point of evidence accumulation, and the time needed for other non-decisional processes. The present study primarily investigated the drift rate differences in different conditions, while the rest of the parameters were not examined and were assumed to be invariable overall. The purpose was to ensure the analyses to be concentrated and simplified as possible, but it was also partly due to the lack of effective way to quantify these parameters directly with the current design. Unlike the drift rate that closely associated with the continuous sensory inputs, the remaining parameters are more dependent to discrete qualitative factors. For example, the decisional boundary would vary between employing speed-driven and accuracy-driven response strategies (Ratcliff & McKoon, 2008; Voss et al., 2004); the starting point can be influenced by the reward history and trial sequences (Nguyen, Josić, & Kilpatrick, 2019); the non-decision time have been suggested related to some physiological individual differences such as age and grey matter volumes in the prefrontal regions (e.g., Ong et al., 2016; Spaniol, Madden, &

Voss, 2006; Spaniol, Voss, & Grady, 2008; Soares et al., 2018). The precise effects from these discrete factors are difficult to be digitised into numeric parameter values.

Since no explicit manipulation on these parameters was introduced in the present experiment design, the assumption about their overall invariance should be reasonable. Even so, the inability in modeling these parameters made the interpretations about the DDM incomplete. In fact, several attempts, such as response-locked analyses and the explorations on the P3 component, were made in the initial plans in order to precisely pinpoint the evidence accumulation interval for each participant, but all of them failed to provide reasonable accounts for the unmodelled parameters. The lack of reliable non-decision time measurement stalled us from dissociating how long the decisional evidence accumulation should last, whereas the absence of decisional boundary values made us hard to tell when exactly the evidence accumulation started and ended. As a result, although many useful information still got revealed based on the drift rates alone, the data fitting quality in the present study was very restricted, and the practical value of the present findings as a predictive computational model was limited. For future studies, these parameters may be able to be measured by incorporating different recording and analysis methods. For example, some studies had suggested that the decisional boundary could be quantified by neuron firing rates in some critical cortices via single-cell recording (e.g., Gold & Shadlen, 2001; Huk & Shadlen, 2005). Other works in the field of computer science and mathematics showed the potential of applying machine learning algorithms to find the optimal estimations of these diffusion model parameters (Vandekerckhove & Tuerlinckx, 2007).

4.6.3. Holism vs. Reductionism.

Last but not least, a more general issue was the reductionism in the theories of the flanker effect. Both the DDM and the CFM studied the flanker effect from a differential approach, which treated the role of each stimulus (target or flanker) as an isolated part and assumed some simple linear relationships between them when contributing to the decision or response. Such a view ignores the potential effects of the whole stimulus array as a holistic entity in cognitive processing, which is alternatively emphasised in a Gestaltism approach. The Gestalt theories particularly argue for a strongly rooted tendency of visual grouping and creating configurations when multiple stimuli are simultaneously presented (Wertheimer, 2000).

Without suggesting the reductionist theories to be incorrect, it would be beneficial to address that the cognitive processes in a flanker task can be affected not only by each stimulus separately but also by the entire array as a whole. Although few studies in the recent decades focused on the Gestalt theories, many fundamental principles, such as the laws of proximity, similarity, and closure, could well apply to the perceptual recognitions and judgements in the flanker task, at least to some extent. For example, the array in a congruent trial will be more likely to be perceived as an integrated entity because of the spatial identity of stimuli, but such integration may be broken in an incongruent trial since the target becomes visually distinguished from the flankers. These effects are probably more obvious when the task function of a stimulus rely on its spatial properties (e.g., shape) rather than the semantics (e.g., correspondent meaning) (Overvliet & Sayim, 2016; Rouder & King, 2003). Future works may be able to investigate these effects in detail and make improvements to the flanker effect theories.

5. Conclusion

In the present study, I examined two theoretical models of the flanker congruency effect, namely the continuous-flow model (CFM) and the drift-diffusion model (DDM), using EEG-based neural indicators. For the CFM, the lateralized readiness potential (LRP) was recorded, and the "Gratton dip" component in the incongruent condition was particularly investigated. For the DDM, the drift rate was calculated as an index of the sensory evidence accumulation rate based on the time-frequency power tagging to the flashing rates of the target and flanker stimuli. Results in the LRP failed to reveal the "Gratton dip" in response to incompatible flankers, but instead observed a significantly delayed peak in the incongruent condition. On the other hand, the drift rate calculated at occipital electrodes (centred on Oz) for this condition was notably lower than for the compatible condition. Both the delayed LRP peak and the slowed drift rate were significantly correlated with response time. Overall, results from the present study provide more support for the DDM in which flanker interference arises at sensory levels of processing rather than at the level of response selection. Nonetheless, the examination method used in this study was still a primitive attempt at this question, and several potential limitations and defects might have impacts on my results and arguments. Further investigations with methodological improvements are needed to get more comprehensive knowledge on the neural bases underlying the flanker congruency effect.

6. Appendices

Appendix A: ANOVA & Pairwise Comparison Result Tables of Behavioural ACC and RT.

Table 3.
2 × 3 repeated-measure ANOVA results on behavioural accuracy (ACC) and response time (RT).

Measure	Predictor	*df*	SS	MS	*F*	*p*	η_p^2
ACC	Congruency	1	.042	.042	24.840	<.001 ***	.479
	Flicker	2	.002	.001	3.563	<.05 *	.117
	Congruency × Flicker	2	.000	.000	.766	.470	.028
	Error	27	.103	.004			
RT (ms)	Congruency	1	49223	49223	210.6	<.001 ***	.886
	Flicker	2	1134	566.9	6.991	<.01 **	.206
	Congruency × Flicker	2	161	80.34	1.209	.307	.043
	Error	27	904777	33510			

Note. ACC = Accuracy; RT = Response time, *df* = Degree of freedom; SS = Sum of Squares; MS = Mean Square; η_p^2 = partial η^2. . $p < .1$, * $p < .05$, ** $p < .01$; *** $p < .001$.

Table 4.1.

Pairwise comparisons of behavioural response accuracy (ACC).

Predictor	Contrast	MD	*SE*	*df*	*t*	*p*
Flicker	A - C	.007	.003	54	2.430	<.05 *
	B - C	.007	.003	54	2.172	.085 .
	A - B	.001	.003	54	.257	.964
Congruency	CO - IN	.032	.006	27	4.985	<.001 ***

Table 4.2.

Pairwise comparisons of behavioural response time (RT) (ms).

Predictor	Contrast	MD	*SE*	*df*	*t*	*p*
Flicker	A - C	-2.79	1.7	54	-1.641	.237
	B - C	-6.35	1.7	54	-3.730	<.01 **
	A - B	3.56	1.7	54	2.089	.102
Congruency	CO - IN	-34.2	2.36	27	-14.5110	<.001 ***

Note. MD = Mean difference; *SE* = Standard error; *df* = Degree of freedom. *p* values were corrected by Tukey's HSD test. . $p < .1$, * $p < .05$, ** $p < .01$; *** $p < .001$.

Appendix B: ANOVA & Pairwise Comparison Result Tables of LRP.

Table 5.
2 × 3 repeated-measure ANOVA results on the lateralized readiness potential (LRP) amplitude and latency.

Measure	Predictor	*df*	SS	MS	*F*	*p*	η_p^2
LRP Amplitude (μV)	Congruency	1	.002	.002	.043	.837	.002
	Flicker	2	.042	.021	.848	.434	.030
	Congruency × Flicker	2	.162	.081	3.909	<.05 *	.126
	Error	27	3.018	.112			
LRP Latency (ms)	Congruency	1	134414	134414	30.730	<.001 ***	.532
	Flicker	2	8810	4405	1.013	.370	.036
	Congruency × Flicker	2	5282	2641	1.07	.350	.038
	Error	27	237168	8784			

Note. df = Degree of freedom; SS = Sum of Squares; MS = Mean Square; η_p^2 = partial η^2. . $p < .1$, * $p < .05$, ** $p < .01$; *** $p < .001$.

Table 6.1.
Pairwise comparisons of lateralized readiness potential (LRP) amplitude (μV) between flicker × congruency conditions.

Predictor	Contrast	MD	*SE*	*df*	*t*	*p*
Flicker × Congruency	ACO - CCO	.035	.040	107	.878	.655
	BCO - CCO	.030	.040	107	.744	.738
	ACO - BCO	.005	.040	107	.134	.990
	AIN - CIN	-.113	.040	107	-2.801	<.05 *
	BIN - CIN	-.072	.040	107	-1.795	.176
	AIN - BIN	-.041	.040	107	-1.006	.575

Table 6.2.
Pairwise comparisons of lateralized readiness potential (LRP) latency (ms) between congruency conditions.

Predictor	Contrast	MD	*SE*	*df*	*t*	*p*
Congruency	CO - IN	-56.571	10.205	27	-5.543	<.001 ***

Note. MD = Mean difference; *SE* = Standard error; *df* = Degree of freedom. *p* values were corrected by Tukey's HSD test. . $p < .1$, * $p < .05$, ** $p < .01$; *** $p < .001$.

Appendix C: ANOVA & Pairwise Comparison Result Tables of ERP.

Table 7.
2 × 3 repeated-measure ANOVA results on the ERP components at Oz.

Measure	Predictor	*df*	SS	MS	*F*	*p*	η_p^2
$N1_{Oz}$ Amplitude (μV)	Congruency	1	.147	.147	1.531	.227	.054
	Flicker	2	29.49	14.744	41.81	<.001 ***	.608
	Congruency × Flicker	2	.007	.004	.033	.968	.001
	Error	27	679.9	25.18			
$P2_{Oz}$ Amplitude (μV)	Congruency	1	.190	.190	1.861	.184	.064
	Flicker	2	3.872	1.936	10.98	<.001 ***	.289
	Congruency × Flicker	2	.057	.028	.638	.532	.023
	Error	27	470.9	17.44			
$P3_{Oz}$ Amplitude (μV)	Congruency	1	.509	.509	3.76	.063 .	.122
	Flicker	2	.085	.043	.644	.529	.023
	Congruency × Flicker	2	.050	.025	.889	.417	.031
	Error	27	101.2	3.747			
$P3_{Oz}$ Latency (ms)	Congruency	1	1090	1090	1.077	.309	.038
	Flicker	2	378	189.2	.339	.714	.012
	Congruency × Flicker	2	368	184.1	.477	.623	.017
	Error	27	318046	11779			
$P3_{Oz}$ Maximum (μV)	Congruency	1	.002	.002	.006	.94	.001
	Flicker	2	.396	.198	1.251	.294	.044
	Congruency × Flicker	2	.231	.115	1.538	.224	.054
	Error	27	392.7	14.54			
$P3_{Oz}$ Duration (ms)	Congruency	1	2752	2752.4	2.834	.104	.095
	Flicker	2	1586	793.2	1.894	.16	.066
	Congruency × Flicker	2	205	102.4	0.262	.771	.010
	Error	27	201819	7475			

Note. df = Degree of freedom; SS = Sum of Squares; MS = Mean Square; η_p^2 = partial η^2. . $p < .1$, * $p < .05$, ** $p < .01$; *** $p < .001$.

Table 8.
2 × 3 repeated-measure ANOVA results on the ERP components at Pz.

Measure	Predictor	*df*	SS	MS	*F*	*p*	η_p^2
$N1_{Pz}$ Amplitude (μV)	Congruency	1	.162	.162	1.952	.174	.067
	Flicker	2	7.151	3.576	22.43	<.001 ***	.454
	Congruency × Flicker	2	.093	.047	.84	.437	.030
	Error	27	217.8	8.066			
$P2_{Pz}$ Amplitude (μV)	Congruency	1	.199	.199	2.901	.1	.097
	Flicker	2	3.944	1.972	18.36	<.001 ***	.405
	Congruency × Flicker	2	.039	.019	.564	.572	.020
	Error	27	378.5	14.02			
$P3_{Pz}$ Amplitude (μV)	Congruency	1	.006	.006	.064	.803	.002
	Flicker	2	.026	.0129	.249	.781	.009
	Congruency × Flicker	2	.0835	.0417	2.229	.118	.076
	Error	27	184.9	6.849			
$P3_{Pz}$ Latency (ms)	Congruency	1	6096	6096	7.814	<.01 **	.224
	Flicker	2	189	94.4	.119	.888	.004
	Congruency × Flicker	2	2848	1424.1	1.462	.241	.051
	Error	27	237244	8787			
$P3_{Pz}$ Maximum (μV)	Congruency	1	2.064	2.064	10.74	<.01 **	.285
	Flicker	2	.063	.032	.346	.709	.013
	Congruency × Flicker	2	.13	.0649	1.067	.351	.038
	Error	27	520.5	19.28			
$P3_{Pz}$ Duration (ms)	Congruency	1	6339	6339	14.62	<.001 ***	.351
	Flicker	2	349	174.4	.324	.724	.012
	Congruency × Flicker	2	453	226.6	1.135	.329	.040
	Error	27	85238	3157			

Note. df = Degree of freedom; SS = Sum of Squares; MS = Mean Square; η_p^2 = partial η^2. . $p < .1$, * $p < .05$, ** $p < .01$; *** $p < .001$.

Table 9.
2 × 3 repeated-measure ANOVA results on the ERP components at CPz.

Measure	Predictor	*df*	SS	MS	*F*	*p*	η_p^2
N1 $_{CPz}$ Amplitude (μV)	Congruency	1	.016	.016	.628	.435	.023
	Flicker	2	1.765	.883	24.62	<.001 ***	.477
	Congruency × Flicker	2	.030	.0148	.694	.504	.025
	Error	27	50.08	1.855			
P2 $_{CPz}$ Amplitude (μV)	Congruency	1	.016	.016	.924	.345	.033
	Flicker	2	.260	.130	4.044	<.05 *	.130
	Congruency × Flicker	2	.009	.004	.256	.775	.009
	Error	27	33.93	1.257			
P3 $_{CPz}$ Amplitude (μV)	Congruency	1	.016	.016	.650	.427	.024
	Flicker	2	.003	.002	.102	.903	.004
	Congruency × Flicker	2	.012	.006	.966	.387	.035
	Error	27	40.41	1.497			
P3 $_{CPz}$ Latency (ms)	Congruency	1	138	137.5	.196	.662	.007
	Flicker	2	2383	1191.5	1.252	.294	.044
	Congruency × Flicker	2	2492	1246	.782	.462	.028
	Error	27	226120	8375			
P3 $_{CPz}$ Maximum (μV)	Congruency	1	.269	.269	4.703	<.05 *	.148
	Flicker	2	.012	.006	.197	.822	.007
	Congruency × Flicker	2	.001	.001	.033	.968	.001
	Error	27	106.9	3.958			
P3 $_{CPz}$ Duration (ms)	Congruency	1	3810	3810	2.297	.141	.078
	Flicker	2	141	70.6	.055	.947	.002
	Congruency × Flicker	2	737	368.7	.345	.71	.013
	Error	27	246223	9119			

Note. df = Degree of freedom; SS = Sum of Squares; MS = Mean Square; η_p^2 = partial η^2. . $p < .1$, * $p < .05$, ** $p < .01$; *** $p < .001$.

Table 10.1.
Pairwise comparisons of $N1_{Oz}$ Amplitude (μV) between flicker conditions.

Predictor	Contrast	MD	*SE*	*df*	*t*	*p*
Flicker	A - C	.104	.112	54	.929	.624
	B - C	-.832	.112	54	-7.414	<.001 ***
	A - B	.936	.112	54	8.343	<.001 ***

Table 10.2.
Pairwise comparisons of $P2_{Oz}$ Amplitude (μV) between flicker conditions.

Predictor	Contrast	MD	*SE*	*df*	*t*	*p*
Flicker	A - C	-.038	.079	54	-.478	.882
	B - C	.301	.079	54	3.799	<.01 **
	A - B	-.339	.079	54	-4.277	<.001 ***

Table 10.3.
Pairwise comparisons of $P3_{Oz}$ Amplitude (μV) between congruency conditions.

Predictor	Contrast	MD	*SE*	*df*	*t*	*p*
Congruency	CO - IN	-.110	.0568	27	-1.939	.063 .

Note. MD = Mean difference; *SE* = Standard error; *df* = Degree of freedom. *p* values were corrected by Tukey's HSD test. . $p < .1$, * $p < .05$, ** $p < .01$; *** $p < .001$.

Table 11.1.
Pairwise comparisons of N1 $_{Pz}$ Amplitude(μV) between flicker conditions.

Predictor	Contrast	MD	*SE*	*df*	*t*	*p*
Flicker	A - C	.102	.076	54	1.358	.370
	B - C	-.377	.076	54	-5.001	<.001 ***
	A - B	.480	.076	54	6.359	<.001 ***

Table 11.2.
Pairwise comparisons of P2 $_{Pz}$ Amplitude (μV) between flicker conditions.

Predictor	Contrast	MD	*SE*	*df*	*t*	*p*
Flicker	A - C	-.002	.062	54	-.028	.999
	B - C	.324	.062	54	5.233	<.001 ***
	A - B	-.326	.062	54	-5.262	<.001 ***

Table 11.3.
Pairwise comparisons of P3 $_{Pz}$ Latency (ms) between congruency conditions.

Predictor	Contrast	MD	*SE*	*df*	*t*	*p*
Congruency	CO - IN	-12.0	4.31	27	-2.795	<.01 **

Table 11.4.
Pairwise comparisons of P3 $_{Pz}$ Maximum (μV) between congruency conditions.

Predictor	Contrast	MD	*SE*	*df*	*t*	*p*
Congruency	CO - IN	.222	.068	27	3.277	<.01 **

Table 11.5.
Pairwise comparisons of P3 $_{Pz}$ Duration (ms) between congruency conditions.

Predictor	Contrast	MD	*SE*	*df*	*t*	*p*
Congruency	CO - IN	-12.3	3.21	27	-3.823	<.001 ***

Note. MD = Mean difference; *SE* = Standard error; *df* = Degree of freedom. *p* values were corrected by Tukey's HSD test. . $p < .1$, * $p < .05$, ** $p < .01$; *** $p < .001$.

Table 12.1.
Pairwise comparisons of $N1_{CPz}$ Amplitude (μV) between flicker conditions.

Predictor	Contrast	MD	*SE*	*df*	*t*	*p*
Flicker	A - C	.034	.036	54	.940	.6173
	B - C	-.199	.036	54	-5.552	<.001 ***
	A - B	.232	.036	54	6.492	<.001 ***

Table 12.2.
Pairwise comparisons of $P2_{CPz}$ Amplitude (μV) between flicker conditions.

Predictor	Contrast	MD	*SE*	*df*	*t*	*p*
Flicker	A - C	.012	.034	54	.344	.9369
	B - C	.089	.034	54	2.617	<.05 *
	A - B	-.077	.034	54	-2.273	.0684

Table 12.3.
Pairwise comparisons of $P3_{CPz}$ Maximum (μV) between congruency conditions.

Predictor	Contrast	MD	*SE*	*df*	*t*	*p*
Congruency	CO - IN	.08	.0369	27	2.169	<.05 *

Note. MD = Mean difference; *SE* = Standard error; *df* = Degree of freedom. *p* values were corrected by Tukey's HSD test. . $p < .1$, * $p < .05$, ** $p < .01$; *** $p < .001$.

Appendix D: t-test Result Tables of Time-Frequency Differences.

Table 13.
One-sample t-test results on the mean time-frequency differences (TFDs) in each time bin at the target-tagging frequency at electrode Oz.

Time Bin	Condition	Mean	*SD*	*df*	*t*	*p*	*Cohen's d*
0-100 ms	ACO	.029	.128	27	1.204	.120	.228
	AIN	-.010	.171	27	-.316	.623	-.060
	CCO	.015	.159	27	.501	.310	.095
	CIN	.004	.132	27	.175	.431	.033
100-200 ms	ACO	.098	.107	27	4.842	<.001 ***	.915
	AIN	.036	.161	27	1.167	.127	.221
	CCO	.156	.191	27	4.310	<.001 ***	.815
	CIN	.149	.202	27	3.901	<.001 ***	.737
200-300 ms	ACO	.207	.246	27	4.458	<.001 ***	.842
	AIN	.191	.232	27	4.348	<.001 ***	.822
	CCO	.338	.393	27	4.545	<.001 ***	.859
	CIN	.340	.381	27	4.717	<.001 ***	.892
300-400 ms	ACO	.266	.391	27	3.595	<.001 ***	.679
	AIN	.304	.355	27	4.521	<.001 ***	.854
	CCO	.454	.607	27	3.961	<.001 ***	.749
	CIN	.471	.579	27	4.304	<.001 ***	.813
400-500 ms	ACO	.245	.435	27	2.979	<.01 **	.563
	AIN	.317	.453	27	3.701	<.001 ***	.699
	CCO	.434	.657	27	3.495	<.001 ***	.661
	CIN	.474	.619	27	4.054	<.001 ***	.766

Note. SD = Standard deviation; *df* = Degree of freedom. . $p < .1$, * $p < .05$, ** $p < .01$; *** $p < .001$.

Table 14.
One-sample t-test results on the mean time-frequency differences (TFDs) in each time bin at the flanker-tagging frequency at electrode Oz.

Time Bin	Condition	Mean	*SD*	*df*	*t*	*p*	*Cohen's d*
0-100 ms	ACO	-.015	.164	27	-.483	.683	-.091
	AIN	-.029	.133	27	-1.148	.870	-.217
	CCO	.056	.148	27	1.985	<.05 *	.375
	CIN	-.062	.154	27	-2.146	.980	-.406
100-200 ms	ACO	.060	.145	27	2.195	<.05 *	.415
	AIN	.065	.141	27	2.427	<.05 *	.459
	CCO	.086	.094	27	4.835	<.001 ***	.914
	CIN	-.005	.137	27	-.202	.579	-.038
200-300 ms	ACO	.127	.135	27	4.963	<.001 ***	.938
	AIN	.118	.109	27	5.762	<.001 ***	1.089
	CCO	.110	.123	27	4.734	<.001 ***	.895
	CIN	.059	.112	27	2.764	<.001 ***	.522
300-400 ms	ACO	.098	.127	27	4.109	<.001 ***	.777
	AIN	.132	.107	27	6.541	<.001 ***	1.236
	CCO	.102	.165	27	3.261	<.01 **	.616
	CIN	.078	.103	27	4.017	<.001 ***	.759
400-500 ms	ACO	.098	.110	27	4.746	<.001 ***	.897
	AIN	.143	.129	27	5.872	<.001 ***	1.110
	CCO	.084	.118	27	3.755	<.001 ***	.710
	CIN	.076	.100	27	4.037	<.001 ***	.763

Note. SD = Standard deviation; *df* = Degree of freedom. . $p < .1$, * $p < .05$, ** $p < .01$; *** $p < .001$.

Table 15.
One-sample t-test results on the mean time-frequency differences (TFDs) in each time bin at the target-tagging frequency at electrode Pz.

Time Bin	Condition	Mean	*SD*	*df*	*t*	*p*	*Cohen's d*
0-100 ms	ACO	-.002	.113	27	-.076	.530	-.014
	AIN	-.033	.096	27	-1.820	.960	-.344
	CCO	.004	.147	27	.152	.440	.029
	CIN	.008	.135	27	.315	.378	.060
100-200 ms	ACO	.031	.116	27	1.394	.087 .	.264
	AIN	-.001	.087	27	-.062	.524	-.012
	CCO	.055	.125	27	2.331	<.05 *	.441
	CIN	.080	.141	27	3.012	<.01 **	.569
200-300 ms	ACO	.071	.146	27	2.578	<.01 **	.487
	AIN	.075	.089	27	4.444	<.001 ***	.840
	CCO	.136	.187	27	3.831	<.001 ***	.724
	CIN	.165	.208	27	4.206	<.001 ***	.795
300-400 ms	ACO	.102	.201	27	2.672	<.01 **	.505
	AIN	.122	.151	27	4.257	<.001 ***	.805
	CCO	.209	.283	27	3.921	<.001 ***	.741
	CIN	.211	.273	27	4.081	<.001 ***	.771
400-500 ms	ACO	.070	.207	27	1.797	<.05 *	.340
	AIN	.128	.184	27	3.691	<.001 ***	.697
	CCO	.188	.312	27	3.180	<.01 **	.601
	CIN	.201	.298	27	3.557	<.001 ***	.672

Note. SD = Standard deviation; *df* = Degree of freedom. . $p < .1$, * $p < .05$, ** $p < .01$; *** $p < .001$.

Table 16.
One-sample t-test results on the mean time-frequency differences (TFDs) in each time bin at the flanker-tagging frequency at electrode Pz.

Time Bin	Condition	Mean	*SD*	*df*	*t*	*p*	*Cohen's d*
0-100 ms	ACO	-.016	.127	27	-.666	.744	-.126
	AIN	-.027	.115	27	-1.267	.892	-.239
	CCO	.026	.129	27	1.086	.144	.205
	CIN	-.029	.132	27	-1.153	.870	-.218
100-200 ms	ACO	.045	.132	27	1.790	<.05 *	.338
	AIN	.035	.111	27	1.677	.053 .	.317
	CCO	.040	.106	27	1.974	<.05 *	.373
	CIN	.010	.142	27	.381	.353	.072
200-300 ms	ACO	.083	.127	27	3.466	<.001 ***	.655
	AIN	.077	.113	27	3.610	<.001 ***	.682
	CCO	.054	.094	27	3.040	<.01 **	.575
	CIN	.062	.121	27	2.706	<.01 **	.511
300-400 ms	ACO	.082	.124	27	3.502	<.001 ***	.662
	AIN	.104	.119	27	4.616	<.001 ***	.872
	CCO	.053	.114	27	2.442	<.05 *	.462
	CIN	.078	.087	27	4.728	<.001 ***	.894
400-500 ms	ACO	.070	.143	27	2.599	<.01 **	.491
	AIN	.111	.098	27	5.975	<.001 ***	1.129
	CCO	.028	.093	27	1.590	.062 .	.301
	CIN	.064	.087	27	3.909	<.001 ***	.739

Note. SD = Standard deviation; *df* = Degree of freedom. . $p < .1$, * $p < .05$, ** $p < .01$; *** $p < .001$.

Table 17.
One-sample t-test results on the mean time-frequency differences (TFDs) in each time bin at the target-tagging frequency at electrode CPz.

Time Bin	Condition	Mean	*SD*	*df*	*t*	*p*	*Cohen's d*
0-100 ms	ACO	.014	.087	27	.820	.210	.155
	AIN	-.024	.101	27	-1.236	.886	-.234
	CCO	.022	.106	27	1.118	.137	.211
	CIN	-.003	.119	27	-.110	.543	-.021
100-200 ms	ACO	.054	.098	27	2.920	<.01 **	.552
	AIN	.011	.104	27	.567	.288	.107
	CCO	.065	.105	27	3.275	<.01 **	.619
	CIN	.070	.124	27	2.992	<.01 **	.566
200-300 ms	ACO	.076	.136	27	2.958	<.01 **	.559
	AIN	.075	.110	27	3.641	<.001 ***	.688
	CCO	.156	.180	27	4.588	<.001 ***	.867
	CIN	.170	.173	27	5.200	<.001 ***	.983
300-400 ms	ACO	.104	.206	27	2.659	<.01 **	.503
	AIN	.126	.145	27	4.582	<.001 ***	.866
	CCO	.220	.303	27	3.836	<.001 ***	.725
	CIN	.233	.258	27	4.780	<.001 ***	.903
400-500 ms	ACO	.094	.227	27	2.187	<.05 *	.413
	AIN	.141	.192	27	3.875	<.001 ***	.732
	CCO	.208	.351	27	3.139	<.01 **	.593
	CIN	.222	.318	27	3.686	<.001 ***	.697

Note. SD = Standard deviation; *df* = Degree of freedom. . $p < .1$, * $p < .05$, ** $p < .01$; *** $p < .001$.

Table 18.
One-sample t-test results on the mean time-frequency differences (TFDs) in each time bin at the flanker-tagging frequency at electrode CPz.

Time Bin	Condition	Mean	*SD*	*df*	*t*	*p*	*Cohen's d*
0-100 ms	ACO	.020	.123	27	.838	.205	.158
	AIN	-.026	.120	27	-1.157	.871	-.219
	CCO	.033	.117	27	1.474	.076	.279
	CIN	-.045	.117	27	-2.026	.974	-.383
100-200 ms	ACO	.054	.109	27	2.632	<.01 **	.497
	AIN	.030	.117	27	1.339	.096	.253
	CCO	.048	.107	27	2.386	<.05 *	.451
	CIN	.002	.114	27	.093	.463	.018
200-300 ms	ACO	.075	.102	27	3.910	<.001 ***	.739
	AIN	.054	.112	27	2.576	<.01 **	.487
	CCO	.044	.104	27	2.250	<.05 *	.425
	CIN	.029	.118	27	1.312	.100	.248
300-400 ms	ACO	.064	.097	27	3.493	<.001 ***	.660
	AIN	.071	.121	27	3.117	<.01 **	.589
	CCO	.044	.134	27	1.723	<.05 *	.326
	CIN	.036	.095	27	1.985	<.05 *	.375
400-500 ms	ACO	.068	.105	27	3.408	<.01 **	.644
	AIN	.086	.082	27	5.565	<.001 ***	1.052
	CCO	.032	.119	27	1.403	.086 .	.265
	CIN	.032	.099	27	1.703	.050 .	.322

Note. SD = Standard deviation; *df* = Degree of freedom. . $p < .1$, * $p < .05$, ** $p < .01$; *** $p < .001$.

Appendix E: ANOVA and Pairwise Comparison Result Tables of Drift Rates.

Table 19.
2 × 2 repeated-measure ANOVA results on the drift rates (*v*) at Oz at the early and the late stage.

Measure	Predictor	*df*	SS	MS	*F*	*p*	η_p^2
$v_{\text{Oz - early}}$	Congruency	1	.863	.863	34.001	<.001 ***	.557
	Flicker	2	.606	.606	14.400	<.001 ***	.348
	Congruency × Flicker	2	.067	.067	2.122	.157	.073
	Error	27	4.585	.170			
$v_{\text{Oz - late}}$	Congruency	1	.728	.728	17.39	<.001 ***	.392
	Flicker	2	1.158	1.158	8.735	<.01 **	.244
	Congruency × Flicker	2	.011	.011	.461	.503	.017
	Error	27	25.84	.957			

Note. df = Degree of freedom; SS = Sum of Squares; MS = Mean Square; η_p^2 = partial η^2. . *p* < .1, * *p* < .05, ** *p* < .01; *** *p* < .001.

Table 20.
2 × 2 repeated-measure ANOVA results on the drift rates (*v*) at Pz at the early and the late stage.

Measure	Predictor	*df*	SS	MS	*F*	*p*	η_p^2
$v_{\text{Pz - early}}$	Congruency	1	.252	.252	8.437	<.01 **	.238
	Flicker	2	.124	.124	6.168	<.05 *	.186
	Congruency × Flicker	2	.043	.043	1.222	S.279	.043
	Error	27	1.467	.054			
$v_{\text{Pz - late}}$	Congruency	1	.432	.432	10.256	<.01 **	.275
	Flicker	2	.263	.263	6.771	<.05 *	.200
	Congruency × Flicker	2	.011	.011	.501	.485	.018
	Error	27	5.455	.202			

Note. df = Degree of freedom; SS = Sum of Squares; MS = Mean Square; η_p^2 = partial η^2. . *p* < .1, * *p* < .05, ** *p* < .01; *** *p* < .001.

Table 21.
2 × 2 repeated-measure ANOVA results on the drift rates (v) at CPz at the early and the late stage.

Measure	Predictor	*df*	SS	MS	*F*	*p*	η_p^2
$v_{\text{CPz - early}}$	Congruency	1	.229	.229	10.968	<.01 **	.289
	Flicker	2	.119	.119	9.236	<.01 **	.255
	Congruency × Flicker	2	.040	.040	1.378	.251	.049
	Error	27	1.23	.046			
$v_{\text{CPz - late}}$	Congruency	1	.198	.198	7.146	<.05 *	.209
	Flicker	2	.357	.357	8.751	<.01 **	.245
	Congruency × Flicker	2	.019	.019	.814	.375	.029
	Error	27	6.474	.240			

Note. df = Degree of freedom; SS = Sum of Squares; MS = Mean Square; η_p^2 = partial η^2. . $p < .1$, * $p < .05$, ** $p < .01$; *** $p < .001$.

Table 22.1.
Pairwise comparisons of $v_{Oz\ -\ early}$ between flicker conditions.

Predictor	Contrast	MD	*SE*	*df*	*t*	*p*
Flicker	A - C	-.147	.039	27	-3.795	<.001 ***

Table 22.2.
Pairwise comparisons of $v_{Oz\ -\ late}$ between flicker conditions.

Predictor	Contrast	MD	*SE*	*df*	*t*	*p*
Flicker	A - C	-.203	.069	27	-2.956	<.01 **

Table 22.3.
Pairwise comparisons of $v_{Oz\ -\ early}$ between congruency conditions.

Predictor	Contrast	MD	*SE*	*df*	*t*	*p*
Congruency	CO - IN	.176	.030	27	5.831	<.001 ***

Table 22.4.
Pairwise comparisons of $v_{Oz\ -\ late}$ between congruency conditions.

Predictor	Contrast	MD	*SE*	*df*	*t*	*p*
Congruency	CO - IN	.161	.039	27	4.170	<.001 ***

Note. MD = Mean difference; *SE* = Standard error; *df* = Degree of freedom. *p* values were corrected by Tukey's HSD test. . $p < .1$, * $p < .05$, ** $p < .01$; *** $p < .001$.

Table 23.1.
Pairwise comparisons of $v_{Pz\text{ - }early}$ between flicker conditions.

Predictor	Contrast	MD	*SE*	*df*	*t*	*p*
Flicker	A - C	-.067	.027	27	-2.484	<.05 *

Table 23.2.
Pairwise comparisons of $v_{Pz\text{ - }late}$ between flicker conditions.

Predictor	Contrast	MD	*SE*	*df*	*t*	*p*
Flicker	A - C	-.097	.037	27	-2.602	<.05 *

Table 23.3.
Pairwise comparisons of $v_{Pz\text{ - }early}$ between congruency conditions.

Predictor	Contrast	MD	*SE*	*df*	*t*	*p*
Congruency	CO - IN	.095	.033	27	2.905	<.01 **

Table 23.4.
Pairwise comparisons of $v_{Pz\text{ - }late}$ between congruency conditions.

Predictor	Contrast	MD	*SE*	*df*	*t*	*p*
Congruency	CO - IN	.124	.039	27	3.203	<.01 **

Note. MD = Mean difference; *SE* = Standard error; *df* = Degree of freedom. *p* values were corrected by Tukey's HSD test. . $p < .1$, * $p < .05$, ** $p < .01$; *** $p < .001$.

Table 24.1.
Pairwise comparisons of $v_{CPz - early}$ between flicker conditions.

Predictor	Contrast	MD	*SE*	*df*	*t*	*p*
Flicker	A - C	-.065	.022	27	-3.039	<.01 **

Table 24.2.
Pairwise comparisons of $v_{CPz - late}$ between flicker conditions.

Predictor	Contrast	MD	*SE*	*df*	*t*	*p*
Flicker	A - C	-.113	.038	27	-2.958	<.01 **

Table 24.3.
Pairwise comparisons of $v_{CPz - early}$ between congruency conditions.

Predictor	Contrast	MD	*SE*	*df*	*t*	*p*
Congruency	CO - IN	.091	.027	27	3.312	<.01 **

Table 24.4.
Pairwise comparisons of $v_{CPz - late}$ between congruency conditions.

Predictor	Contrast	MD	*SE*	*df*	*t*	*p*
Congruency	CO - IN	.084	.031	27	2.673	<.01 **

Note. MD = Mean difference; *SE* = Standard error; *df* = Degree of freedom. *p* values were corrected by Tukey's HSD test. . $p < .1$, * $p < .05$, ** $p < .01$; *** $p < .001$.

Appendix F: Ethics Approval.

Office of the Vice-Chancellor

Office of Research Strategy and Integrity (ORSI)

The University of Auckland
Private Bag 92019
Auckland, New Zealand
Level 11, 49 Symonds Street
Telephone: 64 9 373 7599
Extension: 83711
humanethics@auckland.ac.nz

UNIVERSITY OF AUCKLAND HUMAN PARTICIPANTS ETHICS COMMITTEE (UAHPEC)

20-Aug-2019

MEMORANDUM TO:

Assoc Prof Paul Corballis

Psychology

Re: Application for Ethics Approval (Our Ref. 022966): Approved

The Committee considered the application for ethics approval for your study entitled **The electrophysiology of visual cognition**.

We are pleased to inform you that ethics approval has been granted for a period of three years.

The expiry date for this approval is 20-Aug-2022.

Completion of the project: In order that up-to-date records are maintained, you must notify the Committee once your project is completed.

Amendments to the project: Should you need to make any changes to the project, please complete an Amendment Request form in InfoEd, giving full details along with revised documentation. If the project changes significantly, you are required to submit a new application to UAHPEC for approval.

Funded projects: If you received funding for this project, please provide this approval letter to your local Faculty Research Project Coordinator (RPC) or Research Project Manager (RPM) so that the approval can be notified via a Service Request to the Research Operations Centre (ROC) for activation of the grant.

The Chair and the members of UAHPEC would be happy to discuss general matters relating to ethics approvals. If you wish to do so, please contact the Ethics Administrators at humanethics@auckland.ac.nz in the first instance.

Additional information:

1. Do not forget to complete the 'approval wording' on the PISs, CFs and/or advertisements and emails, giving the dates of approval and the reference number. This needs to be completed before you use the documents or send them out to your participants.

Please quote Protocol number **022966** on all communication with the UAHPEC regarding this application.

(This is a computer generated letter. No signature required.)

UAHPEC Administrators

University of Auckland Human Participants Ethics Committee

c.c. Head of Department / School, Psychology

Mr Eric Rosentreter

Kane Pavlovich

Miss Garima Bawa

Tessa Chaffey

Dr Judith Buckley

Miss Laura Jacks

Yichen Qian

Ms Xiao Lin Kee

Miss Sreekari Vogeti

Appendix G: Participant Information Sheet.

PARTICIPANT INFORMATION SHEET

Please retain this information sheet for future reference.

Project title:

The electrophysiology of visual cognition

Principal Investigator/Supervisor:

Associate Professor Paul M. Corballis

Other Researchers:

Jude Buckley, Eric Rosentreter, Steven Qian, Nitish Iyer, Daniele Scanzi, Carley Braddock, Tamar McCambridge

Researcher introduction

This research is being carried out in the School of Psychology at the University of Auckland under the supervision of Associate Professor Paul M. Corballis. I would like to invite you to participate in our research project in the School of Psychology at the University of Auckland. It is important to read this document carefully so that you can make an informed decision about whether you would like to participate.

Research Background

The goal of these experiments is to investigate the neural mechanisms of visual cognition in healthy adults. Your results will help us understand more about how the brain processes visual information.

Procedure

During the experiment you will make simple judgements about visual stimuli presented on a computer monitor. Your responses will be in the form of button presses using the computer keyboard or a button box. You will be given specific instructions at the start of each task.

In addition, your brain waves will be measured during the task using an electroencephalogram (EEG). For EEG, the electrodes will be placed on the surface of your scalp by means of an elastic 'net'. The electrodes are encased in sponges, which are soaked in an electrolyte solution (consisting of shampoo, salt, and water) You will be given brief rest breaks every few minutes during the experiment. Please ask the experimenter any questions that may arise while you are doing the task(s).

We require a total of two hours of your time for this experiment. If you feel any discomfort during the session, please inform the experimenter immediately.

Risks

There are no known risks involved with this experiment beyond those encountered in everyday life. The electrodes and the device used to record your EEG are electrically isolated, so there is no possibility of shock in the unlikely event of an electrical fault in the equipment. The electrode cap is disinfected after each use to prevent the possibility of biological contamination.

Right to Withdraw

You can choose to stop participation at any time without giving a reason. You also have the right to withdraw your data from the research for up to a month after your participation without providing a reason.

Benefits

There is no direct benefit to you by participating in this study, however; your participation will help us to gain a better understanding of the relationships between brain activity and visual cognition.

Koha

If you are participating as part of the School of Psychology Research Participation Scheme, you will receive two hours of credit in return for your participation. If not, you will be given a $20 voucher. If you decide to leave the study early, you will be compensated for the time you participated. You can also request a copy of the final published report of this study.

Confidentiality

Participation in this study is entirely voluntary, and if you choose to participate, you can change your mind at any time without giving a reason and without any negative consequences. Whether you decide to participate in the research or not, it will not influence your relationships with the researchers or the University of Auckland in any way.

After your participation is completed, you will still have the right to request that your data be withdrawn from the study for up to one month. You will be given a copy of this document to keep. The questionnaire responses and other data you provide will be preserved and any information that identifies you as a participant will be used confidentially. Your name will only appear on the attached Consent Form, which will be coded with an identification number that will be used throughout the study. If the information you provide is reported or published, this will be done in a way that does not identify you as its source.

Access to consent forms, questionnaire responses and data will be restricted to the researchers directly involved in this project and will be stored in a locked cabinet on university premises. All data will be kept for a period of six years to allow for publication and future re-analysis, after which it will be securely and confidentially disposed.

Participants will be required to be between 18-60 years of age. Participants with a history of epilepsy or migraine will be excluded, as will participants with uncorrected visual deficits or who experience difficulties in recognising faces or emotional expressions (participants with eyeglasses or contact lenses will be included).

If you would like to participate in this research project, please contact the researcher via email. If you any have questions or concerns about the project, please contact one of the following:

Principal Investigator
Associate Professor Paul M. Corballis
School of Psychology

The Head of School of Psychology
Professor Suzanne Purdy
School of Psychology

The University of Auckland
Private Bag 92019
Auckland 1142
Ph: (09) 3737599 Ext 88562
p.corballis@auckland.ac.nz

The University of Auckland
Private Bag 92019
Auckland 1142
Ph: (09) 3737599 Ext 82073
sc.purdy@auckland.ac.nz

Other Researchers

Jude Buckley jb.h.adv@xtra.co.nz

Eric Rosentreterericthomasrosentreter@gmail.com

Steven Qian yqia803@aucklanduni.ac.nz

Tamar McCambridge tmcc380@aucklanduni.ac.nz

Daniele Scanzi dsca347@aucklanduni.ac.nz

Nitish Iyer niye502@aucklanduni.ac.nz

Carley Braddock cbut010@aucklanduni.ac.nz

For any concerns regarding ethical issues you may contact the Chair, the University of Auckland Human Participants Ethics Committee, at the University of Auckland Research Office, Private Bag 92019, Auckland 1142. Telephone 09 373-7599 ext. 83711. Email: ro-ethics@auckland.ac.nz

Appendix H: Participant Consent Form.

CONSENT FORM

Project title:

The electrophysiology of visual cognition

Principal Investigator/Supervisor:

Associate Professor Paul, M. Corballis

Other Researchers:

Jude Buckley, Eric Rosentreter, Steven Qian, Nitish Iyer, Daniele Scanzi, Carley Braddock, Tamar McCambridge

I have read and understood the accompanying Participant Information Sheet, which explains this research project and my role as a participant. I have had an opportunity to ask questions and have had them answered satisfactorily.

In particular, I understand that:

- I voluntarily agree to take part in this research.
- I will receive either two hours of participation credit or a voucher valued at $20 in return for my participation in this research.
- I have the right to stop participation at any time without having to give a reason.
- Whether or not I participate will not affect my relationship with the researchers or with the University of Auckland.
- For one month after my participation I will still have the right to request that my data be withdrawn from the study.
- My name will appear only on this form. The data from this research will be stored confidentially, coded by number, which will be non-traceable to me.
- All data will be kept for a period of six years to allow for publication and future re-analysis, after which it will be securely and confidentially disposed
- Research publications and presentations from this study will not contain any images information that could identify me without my permission.
- Transcription or analysis of my data will only be conducted by the researchers.
- I consent to have electrodes for EEG attached to my head or face during the experiment
- I wish to receive a summary of findings ☐ Yes ☐ No

  If yes, include an email address that they can be emailed to:

  _____.

Name _____

Signature _____

Date _____

Researcher Use Only

Participant Number

References

Ablin, P., Cardoso, J. F., & Gramfort, A. (2018a). Faster ICA under orthogonal constraint. In *2018 IEEE International Conference on Acoustics, Speech and Signal Processing (ICASSP)* (pp. 4464-4468). IEEE.

Ablin, P., Cardoso, J. F., & Gramfort, A. (2018b). Faster independent component analysis by preconditioning with Hessian approximations. *IEEE Transactions on Signal Processing*, *66*(15), 4040-4049.

Adrian, E. D., & Matthews, B. H. (1934). The Berger rhythm: potential changes from the occipital lobes in man. *Brain*, *57*(4), 355-385.

Alonso-Prieto, E., Van Belle, G., Liu-Shuang, J., Norcia, A. M., & Rossion, B. (2013). The 6 Hz fundamental stimulation frequency rate for individual face discrimination in the right occipito-temporal cortex. *Neuropsychologia*, *51*(13), 2863-2875.

Alós-Ferrer, C. (2018). A Dual-Process Diffusion Model. *Journal of Behavioural Decision Making*, *31*(2), 203-218.

Anderson, J., & Anderson, B. (1993). The myth of persistence of vision revisited. *Journal of Film and Video*, 3-12.

Arnold, N. R., Bröder, A., & Bayen, U. J. (2015). Empirical validation of the diffusion model for recognition memory and a comparison of parameter-estimation methods. *Psychological research*, *79*(5), 882-898.

Averbeck, B. B., Chafee, M. V., Crowe, D. A., & Georgopoulos, A. P. (2003). Neural activity in prefrontal cortex during copying geometrical shapes: I. Single cells encode shape, sequence, and metric parameters. *Experimental brain research*, *150*(2).

Basten, U., Biele, G., Heekeren, H. R., & Fiebach, C. J. (2010). How the brain integrates costs and benefits during decision making. *Proceedings of the National Academy of Sciences*, *107*(50), 21767-21772.

Belliveau, J. W., Kennedy, D. N., McKinstry, R. C., Buchbinder, B. R., Weisskoff, R., Cohen, M. S., ... & Rosen, B. R. (1991). Functional mapping of the human visual cortex by magnetic resonance imaging. *Science*, *254*(5032), 716-719.

Bigdely-Shamlo, N., Kreutz-Delgado, K., Robbins, K., Miyakoshi, M., Westerfield, M., Bel-Bahar, T., ... & Makeig, S. (2013). Hierarchical event descriptor (HED) tags for analysis of event-related EEG studies. In *2013 IEEE Global Conference on Signal and Information Processing* (pp. 1-4). IEEE.

Boucher, L., Palmeri, T. J., Logan, G. D., & Schall, J. D. (2007). Inhibitory control in mind and brain: an interactive race model of countermanding saccades. *Psychological review*, *114*(2), 376.

Brunton, B. W., Botvinick, M. M., & Brody, C. D. (2013). Rats and humans can optimally accumulate evidence for decision-making. *Science*, *340*(6128), 95-98.

Busemeyer, J. R., & Townsend, J. T. (1993). Decision field theory: a dynamic-cognitive approach to decision making in an uncertain environment. *Psychological review*, *100*(3), 432.

Carrillo-De-La-Peña, M., Holguín, S. R., Corral, M., & Cadaveira, F. (1999). The effects of stimulus intensity and age on visual-evoked potentials (VEPs) in normal children. *Psychophysiology*, *36*(6), 693-698.

Colby, C. L., Duhamel, J. R., & Goldberg, M. E. (1996). Visual, presaccadic, and cognitive activation of single neurons in monkey lateral intraparietal area. *Journal of neurophysiology*, *76*(5), 2841-2852.

Coles, M. G., Gratton, G., Bashore, T. R., Eriksen, C. W., & Donchin, E. (1985). A psychophysiological investigation of the continuous-flow model of human information processing. *Journal of Experimental Psychology: Human Perception and Performance*, *11*(5), 529.

Coles, M. G., Scheffers, M. K., & Fournier, L. (1995). Where did you go wrong? Errors, partial errors, and the nature of human information processing. *Acta psychologica*, *90*(1-3), 129-144.

Crick, F., & Koch, C. (1995). Are we aware of neural activity in primary visual cortex?. *Nature*, *375*(6527), 121-123.

Dambacher, M., & Hübner, R. (2013). Investigating the speed–accuracy trade-off: Better use deadlines or response signals?. *Behaviour Research Methods*, *45*(3), 702-717.

Davranche, K., Burle, B., Audiffren, M., & Hasbroucq, T. (2005). Information processing during physical exercise: a chronometric and electromyographic study. *Experimental Brain Research*, *165*(4), 532-540.

Deecke, L., Grözinger, B., & Kornhuber, H. H. (1976). Voluntary finger movement in man: Cerebral potentials and theory. *Biological cybernetics*, *23*(2), 99-119.

Delorme, A., & Makeig, S. (2004). EEGLAB: an open source toolbox for analysis of single-trial EEG dynamics including independent component analysis. *Journal of neuroscience methods*, *134*(1), 9-21.

Diederich, A., & Busemeyer, J. R. (2003). Simple matrix methods for analyzing diffusion models of choice probability, choice response time, and simple response time. *Journal of Mathematical Psychology*, *47*(3), 304-322.

Eimer, M. (1998). The lateralized readiness potential as an on-line measure of central response activation processes. *Behaviour Research Methods, Instruments, & Computers*, *30*(1), 146-156.

Erb, C. D., & Marcovitch, S. (2018). Deconstructing the Gratton effect: Targeting dissociable trial sequence effects in children, pre-adolescents, and adults. *Cognition*, *179*, 150-162.

Erb, C. D., Moher, J., Sobel, D. M., & Song, J. H. (2016). Reach tracking reveals dissociable processes underlying cognitive control. *Cognition*, *152*, 114-126.

Erb, C. D., Moher, J., Song, J. H., & Sobel, D. M. (2018). Reach tracking reveals dissociable processes underlying inhibitory control in 5-to 10-year-olds and adults. *Developmental science*, *21*(2), e12523.

Eriksen, B. A., & Eriksen, C. W. (1974). Effects of noise letters upon the identification of a target letter in a nonsearch task. *Perception & psychophysics*, *16*(1), 143-149.

Eriksen, C. W., & Schultz, D. W. (1979). Information processing in visual search: A continuous flow conception and experimental results. *Perception & psychophysics*, *25*(4), 249-263.

Eriksen, C. W., Coles, M. G., Morris, L. R., & O'hara, W. P. (1985). An electromyographic examination of response competition. *Bulletin of the Psychonomic Society*, *23*(3), 165-168.

Faulkenberry, T. J., Witte, M., & Hartmann, M. (2018). Tracking the continuous dynamics of numerical processing: A brief review and editorial. *Journal of Numerical Cognition*, *4*(2).

Fawcett, I. P., Barnes, G. R., Hillebrand, A., & Singh, K. D. (2004). The temporal frequency tuning of human visual cortex investigated using synthetic aperture magnetometry. *Neuroimage*, *21*(4), 1542-1553.

Fournier, L., Scheffers, M. K., Coles, M. G., Adamson, A., & Abad, E. V. (1997). The dimensionality of the flanker compatibility effect: A psychophysiological analysis. *Psychological Research*, *60*(3), 144-155.

Frank, M. J., Gagne, C., Nyhus, E., Masters, S., Wiecki, T. V., Cavanagh, J. F., & Badre, D. (2015). fMRI and EEG predictors of dynamic decision parameters during human reinforcement learning. *Journal of Neuroscience*, *35*(2), 485-494.

Gawne, T. J., & Martin, J. M. (2002). Responses of primate visual cortical neurons to stimuli presented by flash, saccade, blink, and external darkening. *Journal of neurophysiology*, *88*(5), 2178-2186.

Glimcher, P. W., & Sparks, D. L. (1992). Movement selection in advance of action in the superior colliculus. *Nature*, *355*(6360), 542-545.

Gnadt, J. W., & Andersen, R. A. (1988). Memory related motor planning activity in posterior parietal cortex of macaque. *Experimental brain research*, *70*(1), 216-220.

Gold, J. I., & Shadlen, M. N. (2001). Neural computations that underlie decisions about sensory stimuli. *Trends in cognitive sciences*, *5*(1), 10-16.

Gramfort, A., Luessi, M., Larson, E., Engemann, D. A., Strohmeier, D., Brodbeck, C., ... & Hämäläinen, M. (2013). MEG and EEG data analysis with MNE-Python. *Frontiers in neuroscience*, *7*, 267.

Grandchamp, R., & Delorme, A. (2011). Single-trial normalization for event-related spectral decomposition reduces sensitivity to noisy trials. *Frontiers in psychology*, *2*, 236.

Gratton, G., Coles, M. G., & Donchin, E. (1992). Optimizing the use of information: strategic control of activation of responses. *Journal of Experimental Psychology: General*, *121*(4), 480.

Gratton, G., Coles, M. G., Sirevaag, E. J., Eriksen, C. W., & Donchin, E. (1988). Pre-and poststimulus activation of response channels: a psychophysiological analysis. *Journal of Experimental Psychology: Human perception and performance*, *14*(3), 331.

Hanes, D. P., & Schall, J. D. (1996). Neural control of voluntary movement initiation. *Science*, *274*(5286), 427-430.

Hare, T. A., Schultz, W., Camerer, C. F., O'Doherty, J. P., & Rangel, A. (2011). Transformation of stimulus value signals into motor commands during simple choice. *Proceedings of the National Academy of Sciences*, *108*(44), 18120-18125.

Harlow, I. M., & Donaldson, D. I. (2013). Source accuracy data reveal the thresholded nature of human episodic memory. *Psychonomic Bulletin & Review*, *20*(2), 318-325.

He, S., & Lau, R. W. (2014). Saliency detection with flash and no-flash image pairs. In *European Conference on Computer Vision* (pp. 110-124). Springer, Cham.

Heekeren, H. R., Marrett, S., & Ungerleider, L. G. (2008). The neural systems that mediate human perceptual decision making. *Nature reviews neuroscience*, *9*(6), 467-479.

Heinrich, S. P. (2010). Some thoughts on the interpretation of steady-state evoked potentials. *Documenta Ophthalmologica*, *120*(3), 205-214.

Hermens, F. (2018). When do arrows start to compete? A developmental mouse-tracking study. *Acta Psychologica*, *182*, 177-188.

Herrmann, C. S. (2001). Human EEG responses to 1–100 Hz flicker: resonance phenomena in visual cortex and their potential correlation to cognitive phenomena. *Experimental brain research*, *137*(3), 346-353.

Hillyard, S. A., Hinrichs, H., Tempelmann, C., Morgan, S. T., Hansen, J. C., Scheich, H., & Heinze, H. J. (1997). Combining steady-state visual evoked potentials and f MRI to localize brain activity during selective attention. *Human brain mapping*, *5*(4), 287-292.

Hong, W., Thong, J. Y., & Tam, K. Y. (2004). Does animation attract online users' attention? The effects of flash on information search performance and perceptions. *Information Systems Research*, *15*(1), 60-86.

Horwitz, G. D., & Newsome, W. T. (1999). Separate signals for target selection and movement specification in the superior colliculus. *Science*, *284*(5417), 1158-1161.

Horwitz, G. D., & Newsome, W. T. (2001). Target selection for saccadic eye movements: prelude activity in the superior colliculus during a direction-discrimination task. *Journal of neurophysiology*, *86*(5), 2543-2558.

Hu, L., Xiao, P., Zhang, Z. G., Mouraux, A., & Iannetti, G. D. (2014). Single-trial time–frequency analysis of electrocortical signals: Baseline correction and beyond. *Neuroimage*, *84*, 876-887.

Huart, C., Legrain, V., Hummel, T., Rombaux, P., & Mouraux, A. (2012). Time-frequency analysis of chemosensory event-related potentials to characterise the cortical representation of odors in humans. *PLoS One*, *7*(3), e33221.

Hubel, D. H., & Wiesel, T. N. (1962). Receptive fields, binocular interaction and functional architecture in the cat's visual cortex. *The Journal of physiology*, *160*(1), 106.

Huk, A. C., & Shadlen, M. N. (2005). Neural activity in macaque parietal cortex reflects temporal integration of visual motion signals during perceptual decision making. *Journal of Neuroscience*, *25*(45), 10420-10436.

Hung, C. C., Yen, C. C., Ciuchta, J. L., Papoti, D., Bock, N. A., Leopold, D. A., & Silva, A. C. (2015). Functional mapping of face-selective regions in the extrastriate visual cortex of the marmoset. *Journal of Neuroscience*, *35*(3), 1160-1172.

Isreal, J. B., Chesney, G. L., Wickens, C. D., & Donchin, E. (1980). P300 and tracking difficulty: Evidence for multiple resources in dual-task performance. *Psychophysiology*, *17*(3), 259-273.

Itti, L., & Koch, C. (2001). Computational modelling of visual attention. *Nature reviews neuroscience*, *2*(3), 194-203.

Kappenman, E. S., Farrens, J. L., Zhang, W., Stewart, A. X., & Luck, S. J. (2021). ERP CORE: An open resource for human event-related potential research. *NeuroImage*, *225*, 117465.

Kelly, D. H. (1964). Sine waves and flicker fusion. *Documenta Ophthalmologica*, *18*(1), 16-35.

Kelly, S. P., & O'Connell, R. G. (2013). Internal and external influences on the rate of sensory evidence accumulation in the human brain. *Journal of Neuroscience*, *33*(50), 19434-19441.

Kepecs, A., Uchida, N., Zariwala, H. A., & Mainen, Z. F. (2008). Neural correlates, computation and behavioural impact of decision confidence. *Nature*, *455*(7210), 227-231.

Kiani, R., & Shadlen, M. N. (2009). Representation of confidence associated with a decision by neurons in the parietal cortex. *science*, *324*(5928), 759-764.

Kiani, R., Hanks, T. D., & Shadlen, M. N. (2008). Bounded integration in parietal cortex underlies decisions even when viewing duration is dictated by the environment. *Journal of Neuroscience*, *28*(12), 3017-3029.

Klimesch, W., Fellinger, R., & Freunberger, R. (2011). Alpha oscillations and early stages of visual encoding. *Frontiers in psychology*, *2*, 118.

Kramer, A. F., Wickens, C. D., & Donchin, E. (1985). Processing of stimulus properties: evidence for dual-task integrality. *Journal of Experimental Psychology: Human Perception and Performance*, *11*(4), 393.

Krauzlis, R. J., & Dill, N. (2002). Neural correlates of target choice for pursuit and saccades in the primate superior colliculus. *Neuron*, *35*(2), 355-363.

Kutas, M., & Donchin, E. (1980). Preparation to respond as manifested by movement-related brain potentials. *Brain research*, *202*(1), 95-115.

Laming, D. R. J. (1968). Information theory of choice-reaction times.

Landis, C. (1954). Determinants of the critical flicker-fusion threshold. *Physiological Reviews*, *34*(2), 259-286.

Lee, P. L., Yeh, C. L., Cheng, J. Y. S., Yang, C. Y., & Lan, G. Y. (2011). An SSVEP-*based* BCI using high duty-cycle visual flicker. *IEEE Transactions on Biomedical Engineering*, *58*(12), 3350-3359.

Leite, F. P., & Ratcliff, R. (2011). What cognitive processes drive response biases? A diffusion model analysis. *Judgement & Decision Making*, *6*(7).

Li, Z. (2002). A saliency map in primary visual cortex. *Trends in cognitive sciences*, *6*(1), 9-16.

Lim, S. L., O'Doherty, J. P., & Rangel, A. (2011). The decision value computations in the vmPFC and striatum use a relative value code that is guided by visual attention. *Journal of Neuroscience*, *31*(37), 13214-13223.

Link, S. W., & Heath, R. A. (1975). A sequential theory of psychological discrimination. *Psychometrika*, *40*(1), 77-105.

Miller, J. (1991). The flanker compatibility effect as a function of visual angle, attentional focus, visual transients, and perceptual load: A search for boundary conditions. *Perception & psychophysics*, *49*(3), 270-288.

Morgan, S. T., Hansen, J. C., & Hillyard, S. A. (1996). Selective attention to stimulus location modulates the steady-state visual evoked potential. *Proceedings of the National Academy of Sciences*, *93*(10), 4770-4774.

Mulder, M. J., Van Maanen, L., & Forstmann, B. U. (2014). Perceptual decision neurosciences–a model-based review. *Neuroscience*, *277*, 872-884.

Mullen, T. (2012). CleanLine EEGLAB plugin. *San Diego, CA: Neuroimaging Informatics Toolsand Resources Clearinghouse (NITRC)*.

Müller, M. M., & Hübner, R. (2002). Can the spotlight of attention be shaped like a doughnut? Evidence from steady-state visual evoked potentials. *Psychological science*, *13*(2), 119-124.

Müller, M. M., Andersen, S., Trujillo, N. J., Valdes-Sosa, P., Malinowski, P., & Hillyard, S. (2006). Feature-selective attention enhances color signals in early visual areas of the human brain. *Proceedings of the National Academy of Sciences*, *103*(38), 14250-14254.

Müller, M. M., Teder, W., & Hillyard, S. A. (1997). Magnetoencephalographic recording of steadystate visual evoked cortical activity. *Brain topography*, *9*(3), 163-168.

Nguyen, K. P., Josić, K., & Kilpatrick, Z. P. (2019). Optimizing sequential decisions in the drift–diffusion model. *Journal of mathematical psychology*, *88*, 32-47.

Norcia, A. M., Appelbaum, L. G., Ales, J. M., Cottereau, B. R., & Rossion, B. (2015). The steady-state visual evoked potential in vision research: A review. *Journal of vision*, *15*(6), 4-4.

Norcia, A. M., Candy, T. R., Pettet, M. W., Vildavski, V. Y., & Tyler, C. W. (2002). Temporal dynamics of the human response to symmetry. *Journal of Vision*, *2*(2), 1-1.

Nunez, M. D., Vandekerckhove, J., & Srinivasan, R. (2017). How attention influences perceptual decision making: Single-trial EEG correlates of drift-diffusion model parameters. *Journal of mathematical psychology*, *76*, 117-130.

O'connell, R. G., Dockree, P. M., & Kelly, S. P. (2012). A supramodal accumulation-to-bound signal that determines perceptual decisions in humans. *Nature neuroscience*, *15*(12), 1729-1735.

Ong, G., Sewell, D. K., Weekes, B., McKague, M., & Abutalebi, J. (2017). A diffusion model approach to analysing the bilingual advantage for the Flanker task: The role of attentional control processes. *Journal of Neurolinguistics*, *43*, 28-38.

Osman, A., Lou, L., Muller-Gethmann, H., Rinkenauer, G., Mattes, S., & Ulrich, R. (2000). Mechanisms of speed–accuracy tradeoff: evidence from covert motor processes. *Biological psychology*, *51*(2-3), 173-199.

Overvliet, K. E., & Sayim, B. (2016). Perceptual grouping determines haptic contextual modulation. *Vision Research*, *126*, 52-58.

Palmer, J., Huk, A. C., & Shadlen, M. N. (2005). The effect of stimulus strength on the speed and accuracy of a perceptual decision. *Journal of vision*, *5*(5), 1-1.

Petsche, H., Kaplan, S., Von Stein, A., & Filz, O. (1997). The possible meaning of the upper and lower alpha frequency ranges for cognitive and creative tasks. *International journal of psychophysiology*, *26*(1-3), 77-97.

Philiastides, M. G., Auksztulewicz, R., Heekeren, H. R., & Blankenburg, F. (2011). Causal role of dorsolateral prefrontal cortex in human perceptual decision making. *Current biology*, *21*(11), 980-983.

Philiastides, M. G., Ratcliff, R., & Sajda, P. (2006). Neural representation of task difficulty and decision making during perceptual categorization: a timing diagram. *Journal of Neuroscience*, *26*(35), 8965-8975.

Picton, T. W., Bentin, S., Berg, P., Donchin, E., Hillyard, S. A., Johnson, R., ... & Taylor, M. J. (2000). Guidelines for using human event-related potentials to study cognition: recording standards and publication criteria. *Psychophysiology*, *37*(2), 127-152.

Pisarchik, A. N., Chholak, P., & Hramov, A. E. (2019). Brain noise estimation from MEG response to flickering visual stimulation. *Chaos, Solitons & Fractals: X*, *1*, 100005.

Platt, M. L., & Glimcher, P. W. (1997). Responses of intraparietal neurons to saccadic targets and visual distractors. *Journal of neurophysiology*, *78*(3), 1574-1589.

Polanía, R., Krajbich, I., Grueschow, M., & Ruff, C. C. (2014). Neural oscillations and synchronization differentially support evidence accumulation in perceptual and value-based decision making. *Neuron*, *82*(3), 709-720.

Polich, J. (2007). Updating P300: an integrative theory of P3a and P3b. *Clinical neurophysiology*, *118*(10), 2128-2148.

Ratcliff, R. (1978). A theory of memory retrieval. *Psychological review*, *85*(2), 59.

Ratcliff, R. (1981). A theory of order relations in perceptual matching. *Psychological Review*, *88*(6), 552.

Ratcliff, R. (1988). Continuous versus discrete information processing: Modeling accumulation of partial information.

Ratcliff, R. (2002). A diffusion model account of response time and accuracy in a brightness discrimination task: Fitting real data and failing to fit fake but plausible data. *Psychonomic bulletin & review*, *9*(2), 278-291.

Ratcliff, R., & Childers, R. (2015). Individual differences and fitting methods for the two-choice diffusion model of decision making. *Decision*, *2*(4), 237.

Ratcliff, R., & McKoon, G. (2008). The diffusion decision model: theory and data for two-choice decision tasks. *Neural computation*, *20*(4), 873-922.

Ratcliff, R., & Rouder, J. N. (1998). Modeling response times for two-choice decisions. *Psychological science*, *9*(5), 347-356.

Ratcliff, R., & Rouder, J. N. (2000). A diffusion model account of masking in two-choice letter identification. *Journal of Experimental Psychology: Human perception and performance*, *26*(1), 127.

Ratcliff, R., & Smith, P. L. (2004). A comparison of sequential sampling models for two-choice reaction time. *Psychological review*, *111*(2), 333.

Ratcliff, R., & Tuerlinckx, F. (2002). Estimating parameters of the diffusion model: Approaches to dealing with contaminant reaction times and parameter variability. *Psychonomic bulletin & review*, *9*(3), 438-481.

Ratcliff, R., Cherian, A., & Segraves, M. (2003). A comparison of macaque behaviour and superior colliculus neuronal activity to predictions from models of two-choice decisions. *Journal of neurophysiology*, *90*(3), 1392-1407.

Ratcliff, R., Philiastides, M. G., & Sajda, P. (2009). Quality of evidence for perceptual decision making is indexed by trial-to-trial variability of the EEG. *Proceedings of the National Academy of Sciences*, *106*(16), 6539-6544.

Ratcliff, R., Smith, P. L., Brown, S. D., & McKoon, G. (2016). Diffusion decision model: Current issues and history. *Trends in cognitive sciences*, *20*(4), 260-281.

Ratcliff, R., Thapar, A., & McKoon, G. (2010). Individual differences, aging, and IQ in two-choice tasks. *Cognitive psychology*, *60*(3), 127-157.

Ratcliff, R., Thapar, A., & McKoon, G. (2011). Effects of aging and IQ on item and associative memory. *Journal of Experimental Psychology: General*, *140*(3), 464.

Ratcliff, R., Van Zandt, T., & McKoon, G. (1999). Connectionist and diffusion models of reaction time. *Psychological review*, *106*(2), 261.

Regan, D. (1966). Some characteristics of average steady-state and transient responses evoked by modulated light. *Electroencephalography and clinical neurophysiology*, *20*(3), 238-248.

Regan, M. P., & Regan, D. (1988). A frequency domain technique for characterising nonlinearities in biological systems. *Journal of theoretical biology*, *133*(3), 293-317.

Roe, R. M., Busemeyer, J. R., & Townsend, J. T. (2001). Multialternative decision field theory: A dynamic connectionst model of decision making. *Psychological review*, *108*(2), 370.

Roitman, J. D., & Shadlen, M. N. (2002). Response of neurons in the lateral intraparietal area during a combined visual discrimination reaction time task. *Journal of neuroscience*, *22*(21), 9475-9489.

Rouder, J. N., & King, J. W. (2003). Flanker and negative flanker effects in letter identification. *Perception & psychophysics*, *65*(2), 287-297.

Sanders, A. F., & Lamers, J. M. (2002). The Eriksen flanker effect revisited. *Acta Psychologica*, *109*(1), 41-56.

Sauseng, P., Klimesch, W., Schabus, M., & Doppelmayr, M. (2005). Fronto-parietal EEG coherence in theta and upper alpha reflect central executive functions of working memory. *International journal of Psychophysiology*, *57*(2), 97-103.

Simonson, E., & Brozek, J. (1952). Flicker fusion frequency: background and applications. *Physiological reviews*, *32*(3), 349-378.

Smid, H. G., Mulder, G., & Mulder, L. J. (1987). The continuous-flow model revisited: perceptual and central motor aspects. *Electroencephalography and Clinical Neurophysiology. Supplement*, *40*, 270-278.

Smulders, F. T., Miller, J. O., & Luck, S. J. (2012). The lateralized readiness potential. *The Oxford handbook of event-related potential components*, 209-229.

Soares, S. M. P., Ong, G., Abutalebi, J., Del Maschio, N., Sewell, D., & Weekes, B. (2019). A diffusion model approach to analyzing performance on the Flanker task: The role of the DLPFC. *Bilingualism: Language and Cognition*, *22*(5), 1194-1208.

Spaniol, J., Madden, D. J., & Voss, A. (2006). A diffusion model analysis of adult age differences in episodic and semantic long-term memory retrieval. Journal of Experimental Psychology: Learning, Memory, and Cognition, 32(1), 101.

Spaniol, J., Voss, A., & Grady, C. L. (2008). Aging and emotional memory: cognitive mechanisms underlying the positivity effect. Psychology and aging, 23(4), 859.

Sparks, D. L. (1999). Conceptual issues related to the role of the superior colliculus in the control of gaze. *Current opinion in neurobiology*, *9*(6), 698-707.

Srinivasan, R., Bibi, F. A., & Nunez, P. L. (2006). Steady-state visual evoked potentials: distributed local sources and wave-like dynamics are sensitive to flicker frequency. *Brain topography*, *18*(3), 167-187.

Stone, M. (1960). Models for choice-reaction time. *Psychometrika*, *25*(3), 251-260.

Suarez, I., Burle, B., Tobon, C., Pineda, D., Lopera, F., Hasbroucq, T., & Casini, L. (2015). Deciphering interference control in adults with ADHD by using distribution analyses and electromyographic activity. *Acta psychologica*, *159*, 85-92.

Tononi, G., Srinivasan, R., Russell, D. P., & Edelman, G. M. (1998). Investigating neural correlates of conscious perception by frequency-tagged neuromagnetic responses. *Proceedings of the National Academy of Sciences*, *95*(6), 3198-3203.

Turner, R., Jezzard, P., Wen, H., Kwong, K. K., Le Bihan, D., Zeffiro, T., & Balaban, R. S. (1993). Functional mapping of the human visual cortex at 4 and 1.5 tesla using deoxygenation contrast EPI. *Magnetic resonance in medicine*, *29*(2), 277-279.

van Dinteren, R., Arns, M., Jongsma, M. L., & Kessels, R. P. (2014). P300 development across the lifespan: a systematic review and meta-analysis. *PloS one*, *9*(2), e87347.

Vandekerckhove, J., & Tuerlinckx, F. (2007). Fitting the Ratcliff diffusion model to experimental data. *Psychonomic bulletin & review*, *14*(6), 1011-1026.

Vogel, E. K., & Luck, S. J. (2000). The visual N1 component as an index of a discrimination process. *Psychophysiology*, *37*(2), 190-203.

Voss, A., Rothermund, K., & Brandtstädter, J. (2008). Interpreting ambiguous stimuli: Separating perceptual and judgemental biases. *Journal of Experimental Social Psychology*, *44*(4), 1048-1056.

Voss, A., Rothermund, K., & Voss, J. (2004). Interpreting the parameters of the diffusion model: An empirical validation. *Memory & cognition*, *32*(7), 1206-1220.

Wagenmakers, E. J., Ratcliff, R., Gomez, P., & McKoon, G. (2008). A diffusion model account of criterion shifts in the lexical decision task. *Journal of memory and language*, *58*(1), 140-159.

Wertheimer,M. (2000). Laws of organization in perceptual forms. InS. Yantis (Ed.), *Visual perception: Essential readings* (pp. 216-224). Philadelphia: Taylor & Francis.

White, C. N., Ratcliff, R., & Starns, J. J. (2011). Diffusion models of the flanker task: Discrete versus gradual attentional selection. *Cognitive psychology*, *63*(4), 210-238.

Wickens, C., Kramer, A., Vanasse, L., & Donchin, E. (1983). Performance of concurrent tasks: a psychophysiological analysis of the reciprocity of information-processing resources. *Science*, *221*(4615), 1080-1082.

Wylie, S. A., Van Den Wildenberg, W. P. M., Ridderinkhof, K. R., Bashore, T. R., Powell, V. D., Manning, C. A., & Wooten, G. F. (2009). The effect of speed-accuracy strategy on response interference control in Parkinson's disease. *Neuropsychologia*, *47*(8-9), 1844-1853.

Zhou, J., Osth, A. F., Lilburn, S. D., & Smith, P. L. (2021). A circular diffusion model of continuous-outcome source memory retrieval: Contrasting continuous and threshold accounts. *Psychonomic Bulletin & Review*, *28*(4), 1112-1130.

Zylberberg, J., Cafaro, J., Turner, M. H., Shea-Brown, E., & Rieke, F. (2016). Direction-selective circuits shape noise to ensure a precise population code. *Neuron*, *89*(2), 369-383.